HYBRID-CAPACITOR WITH POLYANILINE/CARBON ELECTRODES

A Thesis

by

TZU-LING CHEN

Submitted to the Office of Graduate and Professional Studies of
Texas A&M University
in partial fulfillment of the requirements for the degree of

MASTER OF SCIENCE

Chair of Committee,	Yossef A. Elabd
Committee Members,	Jodie L. Lutkenhaus
	Jaime Grunlan
Head of Department,	M. Nazmul Karim

August 2016

Major Subject: Chemical Engineering

ABSTRACT

Hybrid-capacitors have the potential to synergistically combine the benefits of both electrochemical double layer capacitors (EDLCs) (longer cycle life) and pseudo-capacitors (higher capacitance). However, new processes that intimately combine the two primary materials from each capacitor (carbon and conductive polymer, respectively) within the electrodes in an ordered fashion on the nanoscale are needed to realize this potential. In this study, we report on a physical method (simultaneous electrospinning/electrospraying (E/E)) and a chemical method (*in situ* oxidative polymerization) for fabricating hybrid-capacitors with high surface area electrodes consisting of polyaniline (PANI) and carbon materials (referred to as E/E electrodes).

E/E produces a PANI/carbon nanofiber/particle network with fiber diameters in the range of 500 to 2000 nm. The hybrid-capacitor with E/E electrodes exhibits an excellent specific capacitance of 235 F g^{-1} (*vs.* 138 F g^{-1} for capacitor with state-of-the art hybrid electrodes) at a current density of 1 A g^{-1}. Moreover, the capacitor with E/E electrodes retains approximately 84 % capacitance after 1000 charge-discharge cycles (*vs.* 67 % for capacitor with state-of-the art hybrid electrodes). A *post mortem* electron microscopy study of the E/E electrodes provides a rationale for the improved cycling stability. These results demonstrate the feasibility of producing E/E electrodes and their promise as future materials in hybrid-capacitors.

Multiwall carbon nanotube (MWCNT)/PANI composites synthesized *via in situ* oxidative polymerization show improved electrochemical performance in a capacitor

compared with pure MWCNTs due to the compact chemical bonding between MWCNT and PANI. Hybrid-capacitors with E/E MWCNT-PANI composite electrodes were also investigated and showed improved performance. Capacitor performance has a high correlation with morphology and polymer-carbon interface and connectivity and can be modified by fabrication and synthetic processes. A deep fundamental understanding of charge storage mechanisms in hybrid materials will guide the design of future polymer-carbon electrodes for hybrid-capacitors.

TABLE OF CONTENTS

Page

LIST OF FIGURES

Page

LIST OF TABLES

Page

1. INTRODUCTION

1.1 Supercapacitors

Supercapacitors (also known as ultracapacitors or electrochemical capacitors) are energy storage devices designed to bridge a gap between high energy density (specific energy) batteries and high power density (specific power) conventional capacitors. Figure 1.1 shows a Ragone plot (specific power *vs.* specific energy) for a number of different types of energy storage devices.[1] Significant effort has been invested in the development of high-performance lithium-ion batteries; however, lithium-ion batteries still suffer from low specific power and slow discharge rates. The combination of properties from supercapacitors and batteries has the potential significantly improve hybrid-electric and pure electric vehicles, where supercapacitors possess high specific power and fast charging rates and batteries possess high specific energy and slow discharging rates. Currently, supercapacitors have been adopted in various applications, including re-generative breaking in cars, back-up power for energy systems, and in consumer portable electronic devices that require frequent charge-discharge cycling rather than long-term energy storage.

In order to improve supercapacitor performance and meet the requirements of future energy/power demands, finding new materials, new device processing methods, and advancing our understanding of the electrochemical interfaces at the nanoscale are all crucial for the development of advanced supercapacitors.[1] Overall, the fabrication of supercapacitors has two primary goals: (1) to achieve high specific power with rapid and

long-lasting charge-discharge ability, and (2) increasing specific energy density without sacrificing specific power or cycle life. Based on the energy storage mechanism, supercapacitors can be divided into two types: electrochemical double layer capacitors (EDLCs) and pseudo-capacitors.

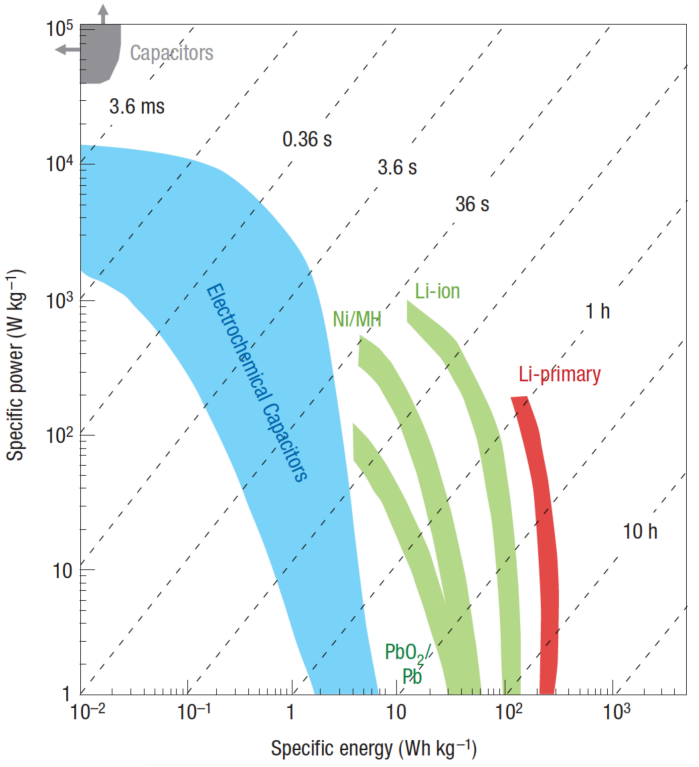

Figure 1.1 Ragone plot (specific power *vs.* specific energy) for various types of energy storage devices. Figure adopted from ref. [1].

1.1.1 Electrochemical Double Layer Capacitors (EDLCs)

EDLCs store energy similar to a traditional capacitor, which is based on an electric double layer concept. Charge is built up in the electrical double layer at the electrode/electrolyte interface.[2] Figure 1.2 shows a schematic of symmetric EDLC, where two electrodes are separated by an ion permeable separator and electrolyte migrates through the separator between the electrodes. When voltage is applied, a layer of positive charge is formed at the internal surface of one electrode, causing the attraction of negative ions from the electrolyte; simultaneously, the internal surface of other electrode forms a layer of negative charge, causing the attraction of positive ions from the electrolyte. Therefore, an electric double layer is formed at the internal electrode surfaces with high capacitance.[3] Since there are no electrochemical reactions between the electrodes, EDLC exhibit fast ion kinetics exclusive to the accessible electrode surface. This charge storage mechanism results in excellent specific power with low energy loss. Since charge storage is exclusive to ion adsorption onto the accessible electrode surface in EDLCs, parameters of importance in electrode materials include porosity and surface area. Carbon materials, in its various forms (*e.g.*, activated carbon, carbon nanotubes, graphene) have been extensively investigated and widely used as EDLC electrodes. Section 1.1.2 provides more information regarding carbon materials as EDLC electrodes. Although various forms of carbon materials have been investigated, the specific energy of EDLCs is still limited by its charge storage mechanism.

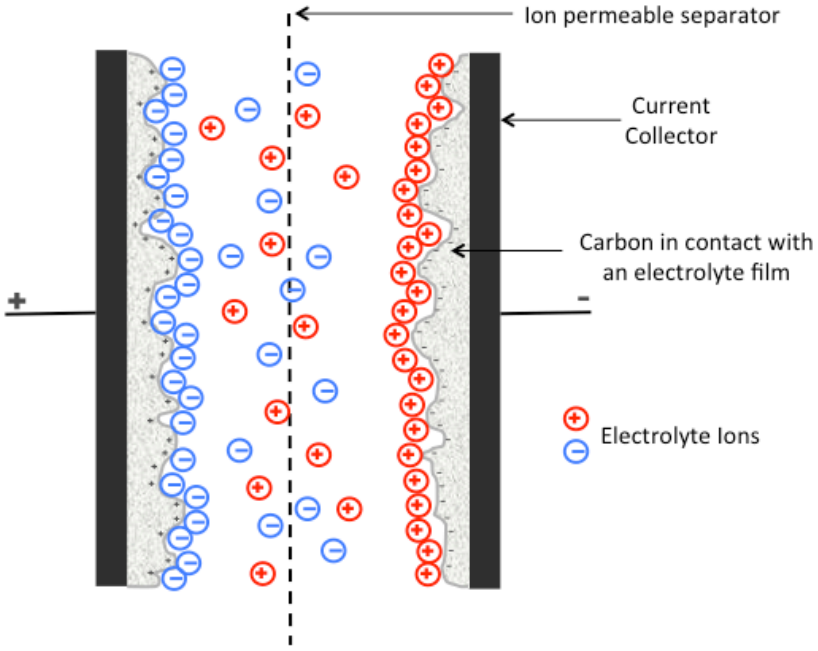

Figure 1.2 Schematic representation of electrochemical double layer capacitor (EDLC).

1.1.2 Pseudo-capacitors

The primary difference between pseudo-capacitors and EDLCs is the process in which charge is stored. Unlike EDLCs, which store charge electrostatically (*i.e.*, ion adsorption), pseudo-capacitors store charge by a Faradaic process, where electrochemical reduction-oxidation (redox) reaction(s) dictate electron charge transfer between electrode and electrolyte.[4] This redox reaction is similar to the electrochemical reaction in rechargeable batteries, where capacitance originates between the extent of charge acceptance (dq) and the charge potential (dV). This ratio dq/dV is called the pseudo-capacitance generated by the redox reaction.[5] This pseudo-capacitance transfer between electrolyte and the electrode surface is accomplished through not only redox

reactions, but also electrosorption and intercalation processes.[6] Figure 1.3 shows a schematic of a pseudo-capacitor, where charge storage is primarily from pseudo-capacitive mechanism (redox reaction(s)), but can still have a small portion from an electrostatic double layer mechanism.[5] Since the reactant molecules in the bulk layer of the pseudo-capacitor can contribute one or more charges on the electrode surface, a pseudo-capacitor system has much higher capacitance than just a double-layer mechanism alone.

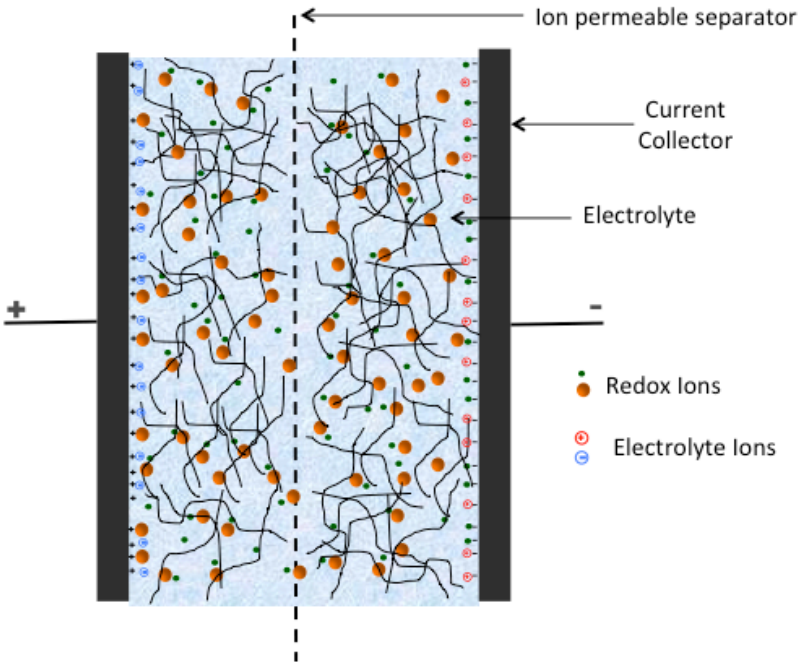

Figure 1.3 Schematic representation of a pseudo-capacitor.

Transition metal oxides and electronically conductive polymers are examples of materials that primarily exhibit pseudo-capacitive behavior. Commonly metal oxides

include ruthenium oxide (RuO_2), manganese oxide (MnO_x), iron oxide (Fe_3O_4), nickel oxide (NiO), while conducting polymers include polyaniline (PANI), polythiophene (PT), polypyrrole (PPy), and other p-conjugated conducting polymers. Although pseudo-capacitors exhibit much higher capacitance compared to EDLCs, they typically have much lower charge-discharge lifetime stability. The redox reactions can degrade polymeric materials resulting in energy loss over time. Therefore, recent studies have focus on combining pseudo-capacitive and electrochemical capacitive materials to generate electrodes with the benefits of both, *i.e.*, hybrid-capacitors.

1.1.3 Hybrid-capacitors

In the past decade, composite materials that combine Faradaic and double layer materials within capacitor electrodes have shown enhanced capacitance and stability (Figure 1.4). This capacitor is referred to as a "hybrid–capacitor" with the advantage of improved specific energy density, while maintaining high specific power.[7] Various complexes include porous carbons with transition metals oxides/hydroxides or conducting polymers. Transition metal oxides/hydroxides can possess great pseudo-capacitance, but also be restricted by limited area, low conductivity, high cost, and toxicity.[8,9] Conductive polymers, with advantages of high specific capacitance, good conductivity, low cost, and ease of fabrication, are gaining interest as one material to incorporate into hybrid capacitors.

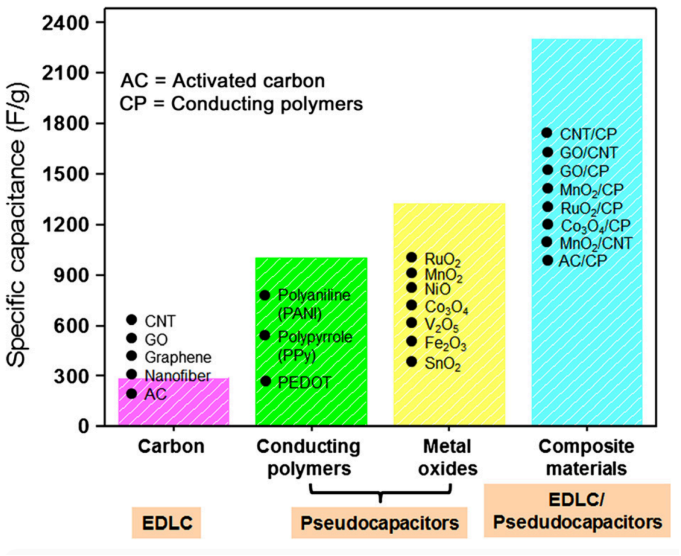

Figure 1.4 Comparison of various electrode materials according to specific capacitance as measured within a capacitor. Figure adopted from ref. [9].

Previous studies have shown the potential of PANI/carbon composite materials as electrodes in hybrid-capacitors.[10-13] Wang *et al.*[12] demonstrated a high specific capacitance of 240 F g^{-1} and 83% capacitance retention after 500 cycles with a hybrid-capacitor with activated carbon-PANI electrodes prepared by electrochemical deposition method. Yan *et al.*[11] fabricated a free-standing, flexible carbon nanotube fiber (CNF)–PANI composite as electrodes and displayed remarkably enhanced electrochemical capacitance compared with the CNF paper. Wang *et al.*[10] demonstrated high capacitance (410 F g^{-1}) and good stability for a capacitor based on cloth-supported single-walled carbon nanotubes (SWCNTs) and PANI nanowire array composite electrodes.

1.2 Materials in Supercapacitors

The goal in supercapacitor fabrication is to improve specific energy without sacrificing high specific power. Therefore, materials with various morphologies have been studied to meet the requirement; recently, materials with specific nanostructures are gaining attention. With their high porosity, greater surface area and flexibility in fabrication process, nanostructured materials have potential in many applications besides supercapacitor, such as chemical sensors, fuel cells and electronic devices. Nanostructured PANI and carbon materials will be discussed in the following sections; two materials that will be the focus of this thesis.

1.2.1 Polyaniline

Polyaniline (PANI), polypyrrole (PPy), and polythiophene (PT) are the most popular conducting polymers used as active electrode materials. These polymers include large π-conjugation length and reversible doping/dedoping ability. Among them, PANI is popular because of its facile doped/undoped structure, high capacitance, good environmental stability, low cost, and good processability.

The basic PANI polymer form is shown in Figure 1.5. It possesses three different states: leucoemeraldine ((1-y)=0), pernigtaniline ((1-y)=1), and emeraldine ((1-y)=0.5).[14]

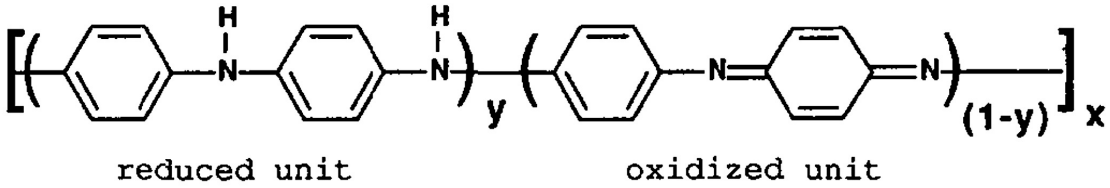

Figure 1.5 General formula of PANI, where $0 \leq (1\text{-}y) \leq 1$. Figure adopted from ref. [14].

The previous two states indicate the fully reduced form (pernigtaniline) and fully oxidized form (leucoemeraldine), which are all poor conductors.[15] Unlike the other two, the partially oxidized emeraldine form in its two states (emeraldine salt (ES) and emeraldine base (EB)) show high conductivity. The transition between EB to ES can be easily controlled *via* an acid-doping process (Figure 1.6). The conductivity of PANI increases reversibly with doping from the undoped base state to the fully doped salt state.[16] This ability makes PANI a promising material for many applications from corrosion protection primer[17,18] to electronic devices.[19]

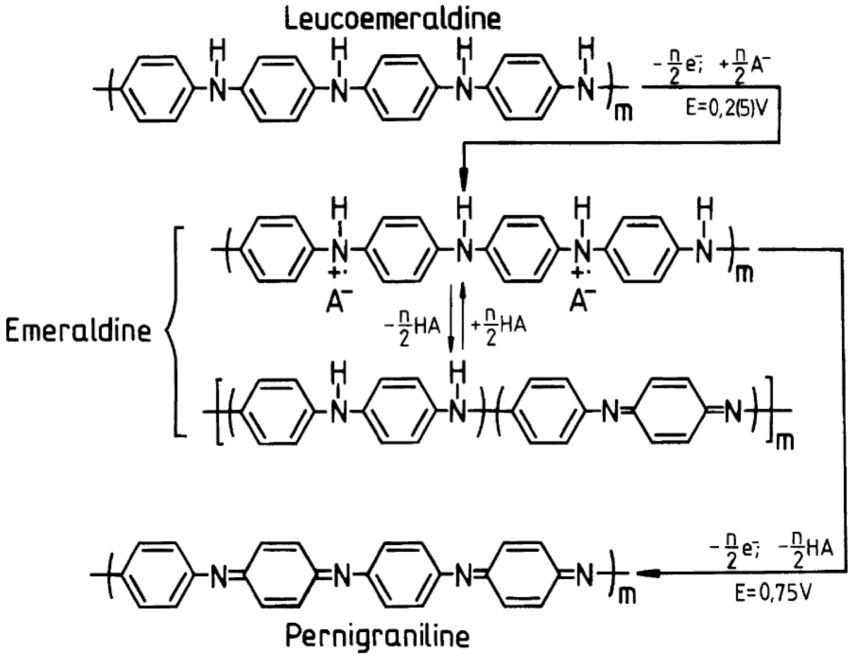

Figure 1.6 Generalized scheme of the oxidative and non-oxidative (protonic acid) doping of PANI. Figure adopted from ref. [19].

Synthesis of PANI can be traced back to the 1980s.[16] The synthesis method can be either chemical oxidation[20] or electrochemical polymerization[21] of the aniline monomer. However, recently with the development of nanotechnology, many studies have been reported for the synthesis PANI with fine nanostructures, such as nanofibers or nanotubes.[22] By modifying the synthesis processing (*e.g.,* acid type, temperature, and material dispersion) the polymer morphology can be easily controlled.[16] In this work, we use chemical oxidation/interfacial polymerization to synthesize PANI.[23] This method can be effective in suppressing secondary growth of PANI and provides the benefit of forming low aspect ratio nanofibers. The polymerization process can be completed in

one step with a wide choice of solvents, acid dopants, and reagents under either room temperature or other temperatures. A detail synthesis process will be provided in section 2.

1.2.2 Carbon Materials

Carbon based materials are popular materials for EDLC electrodes for their low toxicity, stability, high power density, low cost, and easy access. Since only the surface of the electrode contributes to capacitance in EDLCs, various porous carbon materials with high surface area are required. Table 1.1 shows the different carbon used in EDLCs.[24]

Although various advancements have been made in carbon materials, its specific capacitance is still limited by its charge storage mechanism. Therefore, the incorporation of carbon materials with redox-active materials has been explored to improve energy density. In this work, we discuss two different processing methods for combining carbon materials with PANI: a physical method (simultaneously electrospinning/electrospraying) and a chemical method (*in situ* polymerization). The processing details will be discussed in Section 1.3 and Section 3.1.1.

Table.1.1 Different carbon structures used in EDLCs: onion-like carbon, carbon nanotubes, graphene, activated carbon, carbide-derived carbon, and template carbon. Table adopted from ref. [24].

Material	Carbon onions	Carbon nanotubes	Graphene	Activated carbon	Carbide derived carbon	Templated carbon
Dimensionality	0D	1D	2D	3D	3D	3D
Conductivity	High	High	High	Low	Moderate	Low
Volumetric capacitance	Low	Low	Moderate	High	High	Low
Cost	High	High	Moderate	Low	Moderate	High
Structure		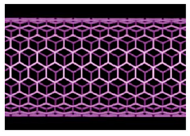	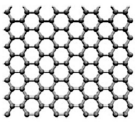	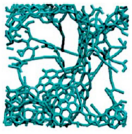	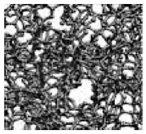	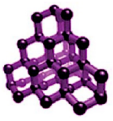

1.3 Electrospinning Method

Electrospinning is a fiber production technique driven by an electric force that can produce polymer fibers with diameters that range from nanometers to several microns. The applications of electrospun fibers include filtration, membranes, tissue engineering, and electronic devices.[25] Liquids for electrospinning usually are polymer solutions or melts. Figure 1.7 shows the fiber formation process through the electrospinning method. When a voltage is applied to the liquid, the liquid becomes charged; an electric repulsive force formed by the electric force counteracts with the surface tension of the liquid. Once at a critical voltage, the liquid is ejected from a needle or surface. With low viscosity, the liquid jet will break up into droplet due to the surface tension resulting in "electrospraying". Contrastingly, for high viscosity liquids, the liquid will not break up, but will travel as a jet to the grounded target resulting in "electrospinning".[26] The quality

and fiber morphology can be controlled by solution parameters and processing parameters. Solution parameters include solution viscosity, conductivity, concentration, and surface tension. Processing parameters include accelerating voltage, needle tip to target distance, humidity, and solution flow rate. There have been a number of studies that have investigated the parameters above in order to understand their relationship between jet instability, bead formation and nanofiber quality.[27-29]

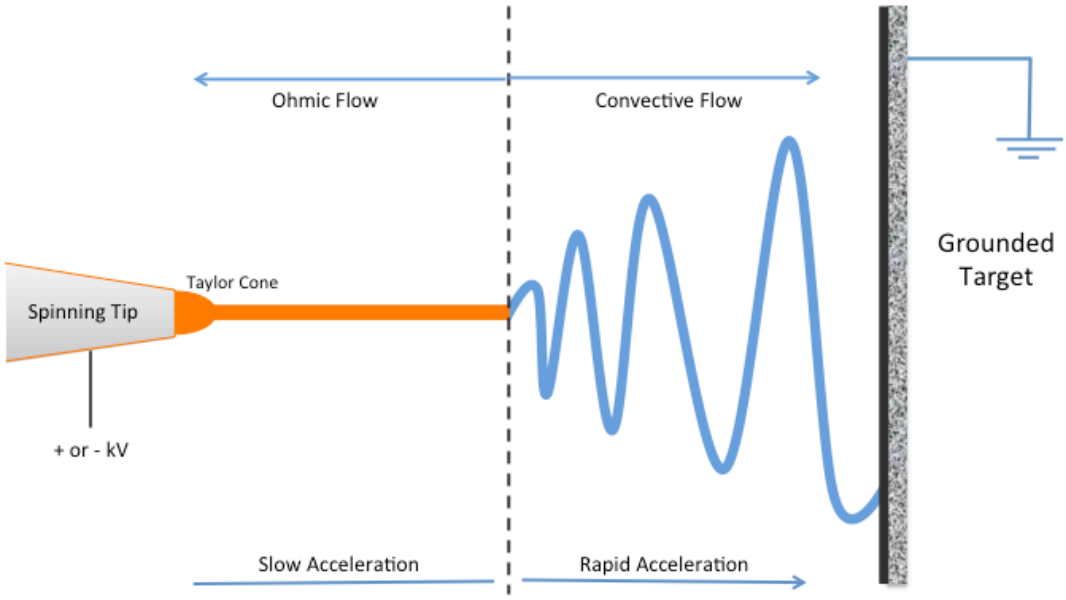

Figure 1.7 Fiber formation *via* electrospinning process.

Recently, ultrafine fibers produced by electrospinning have been applied to electronic devices, such as batteries, supercapacitors, and fuel cells.[25] Previous studies show that porous fiber networks or mats are capable of improving the electrochemical performance

of capacitors.[30-33] The micro-and meso-porous structure of a polymer nanofiber array with small fiber diameters can provide high porosity and large total surface area lower ion and electron resistance.[31] As a simple and inexpensive technique, electrospinning can also be combined with other methods for electrode fabrication. On example of the use of electrospinning to produce capacitor electrodes includes work by Yan *et al.*[11], where they fabricated a flexible carbon nanofiber-polyaniline composite by using rapid-mixture polymerization of aniline in electrospun carbon nanofiber (CNF) paper. The hybrid-capacitor with these electrodes resulted in high capacitance (638 F g^{-1} at 2 A g^{-1}) and good stability (90% capacity retention after 1000 cycles). This is just one example of how electrospinning has become a facile and versatile method to produce nanofibers and can be combined with other processing techniques for a variety of applications where nanostructure can impact performance.[34,35]

1.4 Electrochemical Characterization

Specific capacitance, energy density, power density, and charge-discharge stability are typically used for evaluating capacitor performance. Those parameters can be determined by electrochemical methods: cyclic voltammetry and galvanostatic charge-discharge. In a two-electrode capacitor cell, the total capacitance can be considered as two electrodes in series that can be expressed as follows:

$$\frac{1}{C_T} = \frac{1}{C_n} + \frac{1}{C_p} \tag{1.1}$$

Therefore, for a symmetric capacitor, the two electrodes are identical and the total capacitance will be half of either the negative or positive electrode capacitance. In this study, we used a symmetric cell design as our capacitor.

1.4.1 Cyclic Voltammetry

Cyclic voltammetry (CV) is an electroanalytical technique to study electrode reaction kinetics in electroactive devices.[36] The redox behavior of the device can be observed rapidly over a wide potential range.[37,38] The cyclic voltammogram is obtained by applying a cycling potential to the electrode immersed in an electrolyte and measuring the resulting current. The current is plotted as the function of the applied potential. The testing sample is a working electrode, and the potential of the working electrode is controlled *versus* a reference electrode. The real function of this technique is the analysis of homogeneous chemical reactions that are coupled to the electron transfer process.[39] The coupled chemical reactions are often based on the relative heights of the anodic and cathodic peaks. The important parameters of the cyclic voltammogram are the anodic peak current and cathodic peak current. Detailed background information of CV can be found elsewhere.[29,31,32]

Figure 1.8 shows the cyclic voltammogram of emeraldine base polyanilne in HCl solution.[40] The CV is collected in the potential range of -0.2 to 1 V. Peak no.1 and no.2 are cathodic peaks while peak no.1' and no.2' are corresponding anodic peaks. The peak no.1 associated with the oxidation process of PANI from fully reduced leucoemeraldine to oxidated emeraldine salt; peak no.2 associated with the oxidation process of PANI

from emeraldine base to fully oxidized pernigraniline. The magnitude and position of the redox peaks can change because of different pH, electrolyte, and degradation of materials.[37] In this study, we use CV to compare the electrochemical performance of different electrodes from the magnitude of the redox peaks. The higher redox peaks also indicate the faster ion transfer performance. More information regarding CV experiments will be provided in Section 2.3.2.

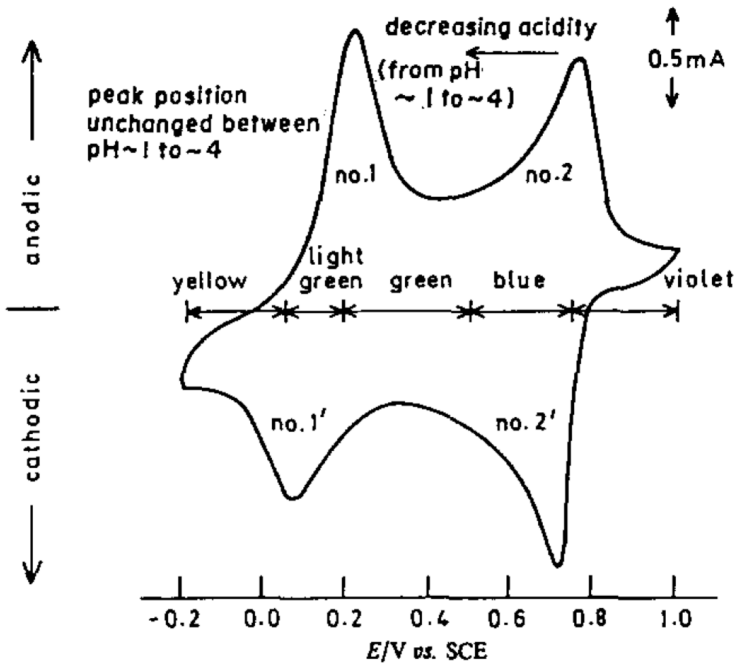

Figure 1.8 Schematic representation of the change in potential of the peaks of the cyclic voltammogram of emeraldine base PANI *vs.* pH (in aqueous HCI). Figure adopted from ref. [40].

1.4.2 Galvanostatic Charge-Discharge and Cycling Stability

The galvanostatic technique, generally called the chronopoentiometric technique, is carried out by applying a controlled current between the working and counter electrode and recording the potential between the working and reference electrode.[37] For a galvanostatic charge-discharge test, the electrode can be charged and discharged under constant current and plotted as potential *versus* time (Figure 1.9). By modifying the charge/discharge current and terminal potential, the time interval for the electrode to reach the terminal potential can be obtained. Specific capacitance (C_{sp}, F g^{-1}) and cell capacitance (C_{cell}, F g^{-1}) can be calculated by following equations:

$$C_{sp} = \frac{I \times \Delta t}{\Delta V \times m} \tag{1.2}$$

$$C_{cell} = 4 \times C_{sp} \tag{1.3}$$

where I is the current density (A), Δt is the discharge time (s), and ΔV is the potential window during the discharge time (s). Based on the C_{sp}, the energy density (E, Wh kg^{-1}), and power density (P, kW g^{-1}) can be calculated from the following equations:

$$E = \frac{1}{2} \times C_{sp} \times V^2 \tag{1.4}$$

$$P = \frac{E}{\Delta t} \times 3.6 \tag{1.5}$$

where V is the potential window (V) and Δt is the discharge time (s).

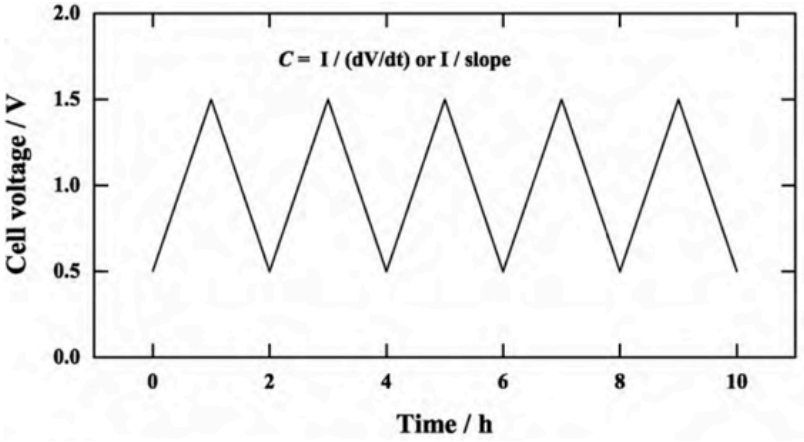

Figure 1.9 Idealized schematic representation of galvanosatic charge-discharge curve. Figure adopted from ref. [1].

Currently, the most important challenge for supercapacitor is to increase the energy density higher than 10 Wh kg^{-1} with low fabrication cost, while using environmentally benign materials. From the equations above, we know that in order to achieve outstanding performance for a supercapacitor, it is critically significant to possess high specific capacitance at a wider operating voltage.[41] The specific capacitance strongly depends on the electrode materials; materials with higher surface area and greater conductivity are ideal. Also, from equation 1.4, the energy density is proportional to the square of operating voltage, which highly affects the energy density. The operating range can be controlled by the choice of electrolyte. For aqueous-based electrolyte, the operating range is limited to <1.2 V, while for non-aqueous-based electrolyte, the operating window can be higher (up to 3.5-4 V). These electrolytes, such as organic

electrolytes and ionic liquids[42,43] have gained interest on increasing the voltage range for supercapacitors.

Cycling stability is significant for supercapacitors to maintain longer performance. For conductive polymers, their structural instability results in volumetric swelling and shrinking during the charge-discharge process that inhibit them from longer performance. Cyclic stability also influences the internal electrode resistance; with high internal resistance, more energy will be wasted to produce unwanted heat during charge-discharge process[44], causing energy loss.

1.5 Outline and Summary

In this study, hybrid-capacitors based on carbon materials and PANI were studied. Our goal is to develop hybrid-capacitors with higher specific capacitance and energy density, while maintaining its excellent power density. Two methods will be presented: simultaneous electrospinning/electrospraying and *in situ* polymerization.

In section2, we demonstrate the use of a simultaneous electrospinning/electrospraying (E/E) process to combine the conductive polymer PANI and porous carbon materials (active carbon/carbon nanotubes). By this method, a unique nanofiber-particle array electrode was produced. This morphology can effectively create higher surface area with more ion adsorption and active porosity for the electrical double layer and charge transfer reactions, resulting in improved capacitor performance. The performance of the E/E hybrid-capacitor was compared with conventional EDLC and pseudo-capacitor and also a hybrid-capacitor that did not use E/E to produce PANI/carbon electrodes. In

section 3, we present a hybrid-capacitor with PANI/multiwall carbon nanotube (MWCNT) electrodes. *In situ* polymerization was utilized to covalently graft PANI unto MWCNTs and this was combined with E/E to produce unique nanofiber-particle PANI-MWCNT array electrodes for hybrid-capacitors. The performance of this PANI-MWCNT E/E hybrid-capacitor was compared to other hybrid-capacitors that did not use E/E or grafting. Overall, the unique morphology of E/E electrodes and their impact on electrochemical performance (capacitor performance and cycling stability) were investigated. Section 4 contains a summary and future outlook for the research presented in this thesis.

2. HYBRID-CAPACITORS WITH POLYANILINE/CARBON ELECTRODES FABRICATED *VIA* SIMULTANEOUS ELECTROSPINNING/ELECTROSPRAYING

2.1 Introduction

Electrospinning is a versatile method in which polymer fibers on the order of less than 100 nm in diameter can be produced by ejecting a polymer solution from a syringe needle under an electric field gradient. Electrodes have been produced with electrospinning for various energy devices, such as batteries, capacitors, and fuel cells.[25,45,46] Previous studies show that carbon fibers produced from the pyrolysis of electrospun polymer fibers can improve capacitor performance.[30-33] The micro-and meso-porous structure of a polymer nanofiber array provides high porosity and large total surface area thereby improving ion absorption and transport, (*i.e.*, higher capacitance and higher ion conductivity).[31,47] Additionally, electrospinning can be combined with other electrode fabrication methods. Several studies combined electrospun materials with polymerization methods[11,13] or with carbonization process[31,48,49]. Studies using electrospinning have already been discussed in Section 1.3.

In this study, we combine electrospinning and electrospraying (E/E) in a simultaneous process to produce PANI/carbon nanofiber/particle electrodes for hybrid-capacitors. The E/E process has been employed previously in our laboratory to produce electrodes for fuel cells[50,51] and reactive membranes for water filtration[52]. Figure 2.1 illustrates the E/E process to produce hybrid electrodes, where this E/E method differs from

electrospinning or electrospraying alone, where nanofibers and particles can form interconnected morphologies simultaneously. This technique provides a facile method to combine fibers/particles in a composite material with tunable particle size, fiber diameter, and material loadings. The electrochemical performance of a hybrid-capacitor with E/E electrodes was evaluated and compared to control capacitors produced with conventional electrode fabrication methods. Morphologies of E/E electrodes before and after capacitor testing was also investigated and compared with conventional electrodes.

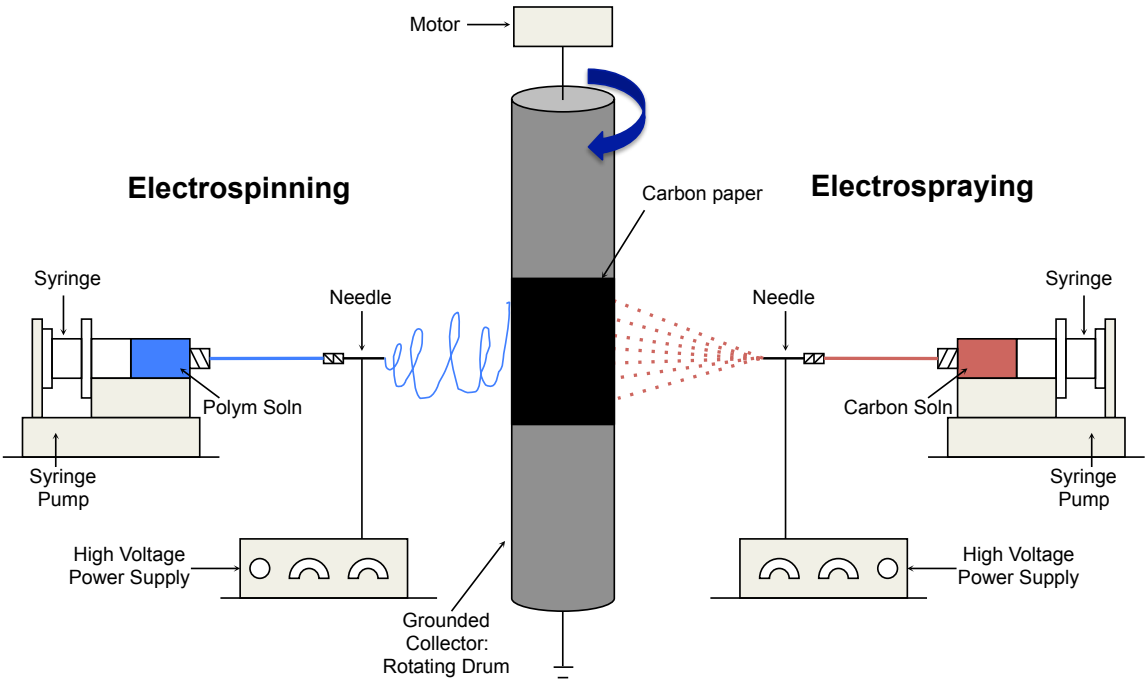

Figure 2.1 Schematic of simultaneous electrospinning/electrospraying (E/E) apparatus.

2.2 Experimental

2.2.1 Materials

Aniline (ACS reagent), chloroform (contains 100-200 ppm amylenes as stabilizer, ≥99.5%), ammonium peroxydisulfate (≥98%), and sulfuric acid (ACS reagent, 95.0-98.0%) were purchased from Sigma-Aldrich and used as received. Polyethylene oxide (PEO, M_w = 8,000,000 g/mol, Polysciences, Inc.), a mixture of activated carbon and carbon nanotubes (activated carbon: APS: 80 nm; carbon nanotube: o.d. = 30-100 nm, length = 5-30 μm, US4898, US Research Nanomaterials), porous separator (25 μm microporous monolayer membrane (PP), 3501, Celgard), and untreated carbon fiber paper (165 μm measured by ultra meter caliper, EC-AC-Paper, FuelCell.com) were used as received. All solutions used in this study were made using deionized water obtained from a NANOPure water purification system (Barnstead) with resistivity greater than 18 MΩ·cm.

2.2.2 Synthesis of Polyaniline

PANI was synthesized by interfacial polymerization using a procedure similar to one previously reported in literature.[20] The procedure is as follows. 3.2 mmol of aniline was dissolved in chloroform. 0.8 mmol of ammonium peroxydisulfate (oxidant) was dissolved in 20 ml of 1 M sulfuric acid. These two solutions were then quickly poured together and formed a two-phase insoluble mixture, where PANI formed at the organic/aqueous interface and diffused into the water phase over a 12 h period at room

temperature. No mechanical stirring was used in the polymerization process. The final product should be dark green in color indicating the emeraldine salt form of PANI. After polymerization, the aqueous phase was collected and purified and mixed in deionized water for 6 h. A dark green PANI powder was obtained after filtering and drying under dynamic vacuum at 40 °C for 24 h.

2.2.3 Fabrication of Electrodes for Capacitors *via* Simultaneous Electrospinning/Electrospraying

The solution for electrospinning was prepared by dissolving PANI in chloroform at 0.67% w/w followed by stirring for 24 h to ensure a clear uniform homogeneous solution. Polyethylene oxide (PEO) was then added to the solution at 0.1% w/w and stirred for 1 h to ensure a uniform solution prior to electrospinning. The electrospraying solution was prepared by adding a mixture of activated carbon and carbon nanotubes to chloroform at 0.7% w/w and sonicating (Q125, QSonica, 125 W, 20 kHz) at an amplitude of 35% for 15 min. Both solutions were placed in two separate glass syringes (CG-3070-03, Chemglass Life Sciences). Figure 2.1 shows a schematic of the simultaneous electrospinnng/electrospraying (E/E) apparatus used to produce the electrodes in this study, which consists of two high-voltage power supplies (PS/EL50R00.8, Glassman High Voltage, Inc. and ES40P-10W/DAM, Gamma High Voltage Research, Inc.), two syringe pumps (NE-1000, New Era Pump Systems), two syringe needles (i.d. = 0.024 in., Hamilton), PTFE tubing (Pt. No. 86510, Hamilton), and a grounded collector (aluminum

foil wrapped cylindrical drum, o.d. = 4.85 cm) connected to a motor (4IK25GN-SW2, Oriental Motor) to allow rotation during the E/E process at 120 rpm. The electrospun fibers and electrosprayed particles were collected on untreated carbon fiber paper, which was adhered to the drum. The solution flow rates, the needle tip to collector distance, and the applied voltage for electrospinning and electrospraying process were 0.5 ml/hr and 1 ml/hr, 7 cm and 10 cm, and 7 kV and, 10 kV, respectively. The E/E electrodes were subsequently annealed at 120 °C for 90 min.

2.2.4 Fabrication of Control Electrodes for Capacitors

The comparative hybrid-capacitor control electrodes were fabricated by solution casting a PANI/carbon solution onto carbon fiber paper. The PANI/carbon solution was a combination of the solutions previously described above (similar to electrospinning and electrospraying solutions). Other controls were also prepared by either solution casting the PANI solution alone (similar to electrospinning solution) on carbon paper to be used in constructing a pseudo-capacitor control or by solution casting the carbon solution alone (similar to electrospraying solution) on carbon paper to be used in constructing an EDLC control. Solutions were transferred from a glass pipet and uniformly drop cast on a 3 x 3 cm carbon fiber paper coupons. The solution-cast samples were then annealed at 80 °C for 5 min. Additional layers were solution cast and annealed until a desired loading of active material of at least 4 mg cm^{-1} was reached. After solution casting a desired amount, all control electrodes were further annealed at 120 °C for 90 min prior to capacitor assembly.

2.2.5 Capacitor Assembly

Symmetrical capacitors were assembled with the electrodes described above in a split test cell (EQ-STC-10, MTI Corporation). Two similar electrodes with similar area (1 cm in diameter) were separated by a porous separator and sandwiched between two stainless steel splits and two or three drops of 1 M sulfuric acid was added as the electrolyte. The same capacitor assembly was used for each set of electrodes. The capacitor produced with E/E electrodes and the ones produced with the three control electrodes will be referred to as (1) E/E hybrid-capacitor, (2) hybrid-capacitor (with solution cast PANI/carbon electrodes), (3) pseudo-capacitor (with solution cast PANI electrodes), and EDLC (with solution cast carbon electrodes).

2.2.6 Capacitor Performance Testing

The capacitor performance of all the four capacitors (E/E hybrid-capacitor and three controls) was measured with a potentiostat/galvanostat (Solartron 1287) with 1 M sulfuric acid as the electrolyte using a two-electrode geometry as described in prior section. Cyclic voltammetry was performed under various scan rates from 50 mV/s to 200 mV/s in the voltage window from -0.2 to 0.8 V. Galvanostatic charge-discharge was performed at various current densities from 0.5 A g^{-1} to 1 A g^{-1} within a 0.9 voltage window. The specific capacitance (C_{sp} [F g^{-1}]) and cell capacitance (C_{cell} [F g^{-1}]) were calculated from the galvanostatic charge-discharge data according to equations 1.2-1.5 in Section 1.4.2.

2.2.7 Electrode Characterization

The morphology of the E/E electrodes was characterized by scanning electron microscopy (SEM; FEI Quanta 600 FE-SEM, 10 kV) under various magnifications. Samples were sputter coated (Cressington 208 HR) with platinum (6 nm thickness) prior to SEM. The PANI loading was measured with thermal gravimetric analysis (TGA; Q50, TA Instrument). A small portion of the electrode (*ca.* 5 - 7 mg) was heated in the TGA from ambient temperature to 900 °C at 10 °C/min in air at 60 ml/min. The PANI loading was calculated by dividing the PANI mass loss by the entire original material mass.

2.3 Results and Discussion

2.3.1 Membrane Morphology

SEM images of the PANI powder, PANI/PEO electrospun fibers, and E/E PANI/carbon composite are shown in Figures 2.2, 2.3, and 2.4, respectively. The SEM image of PANI powder is shown in Figure 2.2, which was prepared by interfacial polymerization in the emeraldine salt form. Agglomerated cylindrical-shaped particles of PANI can be observed with an average sample diameter of 95 nm and diameter distribution range of 80 to 100 nm.

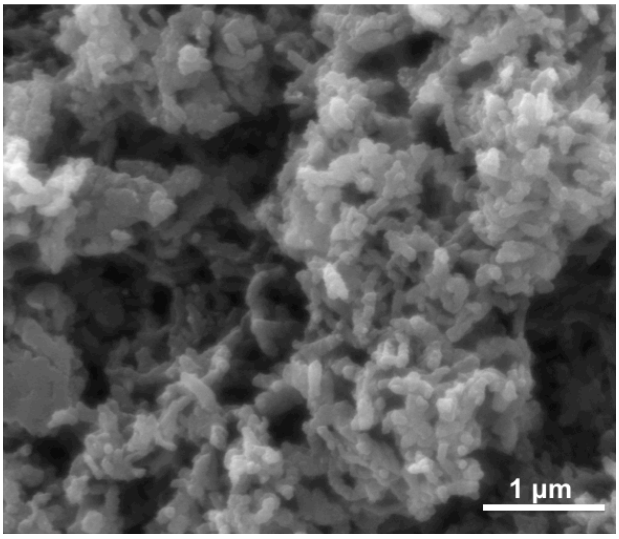

Figure 2.2 SEM image of PANI powder synthesized by interfacial polymerization (X 50000 magnification, scale bar = 1 µm).

Figure 2.3 shows the SEM images of PANI/PEO nanofibers fabricated *via* electrospinning. Highly aligned, straight, and parallel PANI/PEO fiber morphologies were observed, where several large agglomerates (diameter range of 3 to 6 µm) on each fiber can be observed in Figure 2.3(b). The average nanofiber diameter size in Figure 2.3 is 1.67 µm (diameter range of 1 to 4 µm).

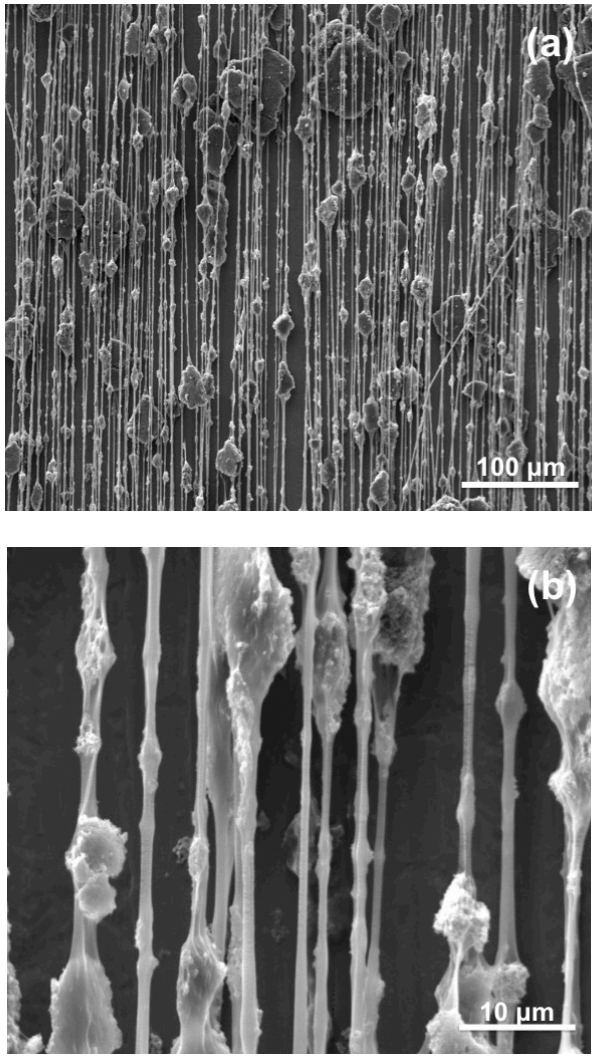

Figure 2.3 SEM images of electrospun PANI/PEO nanofiber mats: (a) X 500 magnification, scale bar = 100 µm; (b) X 5000, scale bar = 10 µm.

Figure 2.4 shows SEM images at various magnifications of PANI/carbon electrode prepared by the E/E method. Figure 2.4(c) shows a magnified view of Figure 2.4(b) with a PANI fiber diameter distribution of 500 to 2000 nm and a carbon particle size distribution of 1 of 5 μm. The carbon particles are finely distributed on the PANI fiber surfaces and form an intimate interconnection between the two materials. This composite structure formed sufficient interspace between each layer providing more surface area comparing with the compact structure prepared by solution casting method (Figure 2.5). The membrane morphology in Figure 2.5 indicates a compact structure with less porosity; in contrast to the solution casting process, the E/E process creates micro- and meso-porous morphology providing more facile access for the electrolyte to react and diffusion throughout electrode.

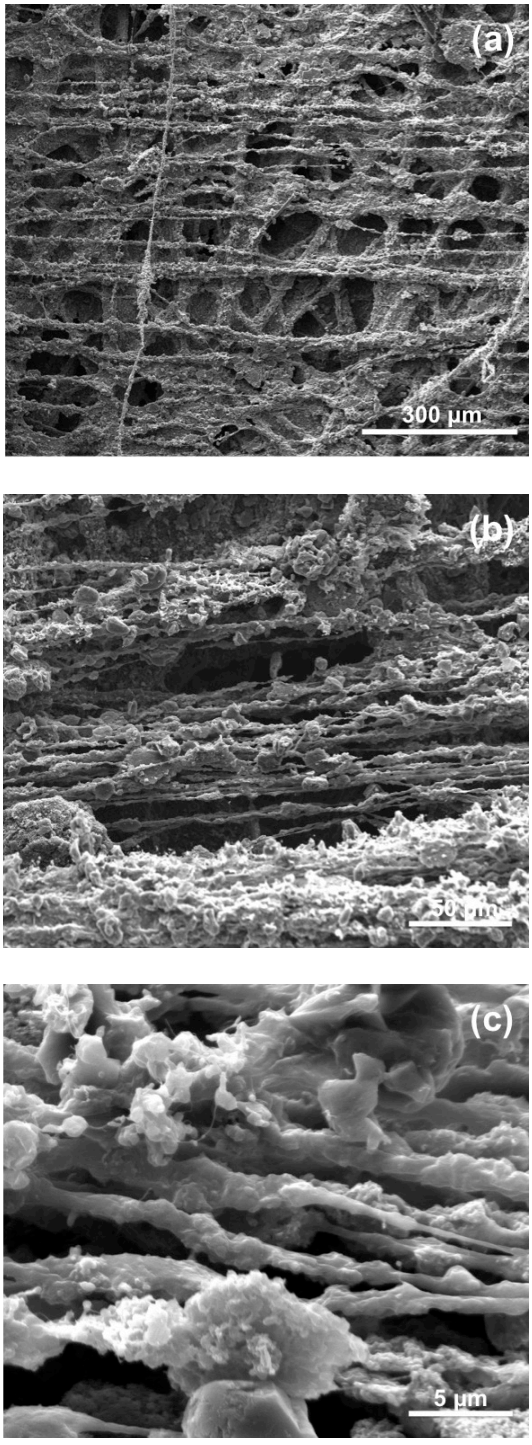

Figure 2.4 SEM images of simultaneous electrospinning/electrospraying PANI/carbon nanocomposite: (a) X 300 magnification, scale bar = 300 µm; (b) X 2000 magnification, scale bar = 40 µm; (c) X 10000 magnification, scale bar = 5 µm.

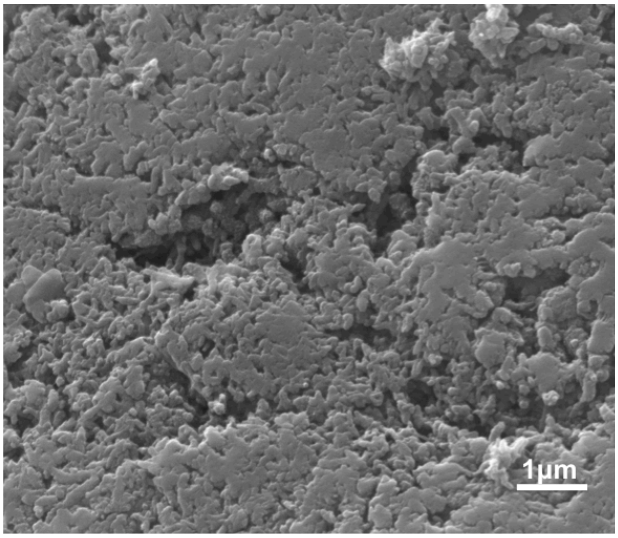

Figure 2.5 SEM images of solution casting PANI/carbon composite: X 30000 magnification, scale bar = 1 µm.

2.3.2 Cyclic Voltammetry and Galvanostatic Charge-Discharge

In order to evaluate the electrochemical properties of E/E hybrid electrodes in a capacitor, the cyclic voltammetry (CV) and galvanostatic charge-discharge of a capacitor with E/E hybrid electrodes (two electrode system) were measured with 1 M H_2SO_4 as the electrolyte. The electrochemical results were compared to control capacitors: EDLC (carbon as the electrodes), pseudo-capacitor (PANI as the electrodes), and hybrid-capacitor (solution cast PANI/carbon as the electrodes). All the testing cells were assembled with a symmetric structure in a split test cell with two 1.57 cm^2 electrodes. Figure 2.6 shows the CV profiles of all four capacitors at a 100 mV s^{-1} scan rate in potential range -0.2 V to 0.8 V. The EDLC shows an expected rectangular profile absent of redox peaks indicative of a typical double layer capacitance performance. Conversely,

the pseudo-capacitor shows two pairs of redox peaks (A/C_1 and A/C_2) corresponding to the transition of PANI between emeraldine/leucoemeraldine and emeraldine/pernigraniline, respectively[53]. Both EDLC and pseudo-capacitor CV behavior shown in Figure 2.6 agree well with literature[54,55]. Among all four capacitors, the pseudo-capacitor exhibits the highest current density, which also corresponds with the highest PANI content. This result is expected and therefore one would expect that a hybrid-capacitor would have a current density higher than the EDLC and lower than the pseudo-capacitor, which is what was observed in Figure 2.6 for both hybrid-capacitors. The E/E hybrid-capacitor, however, has a noticeably higher current density than the conventional hybrid-capacitor. This may be attributed to the interconnected PANI nanostructure that can facilitate more facile electron conduction pathways and charge storage[56]. The morphology change of PANI from powder to fiber form has been shown to result in higher redox peaks[56], indicating faster Faradic reactions at the electrode surface. However, in Figure 2.6, there is no obvious difference in redox peaks between the E/E hybrid-capacitor and the conventional hybrid-capacitor, which may be the result of the addition of the carbon particle morphology and subsequent EDLC charge storage mechanisms.

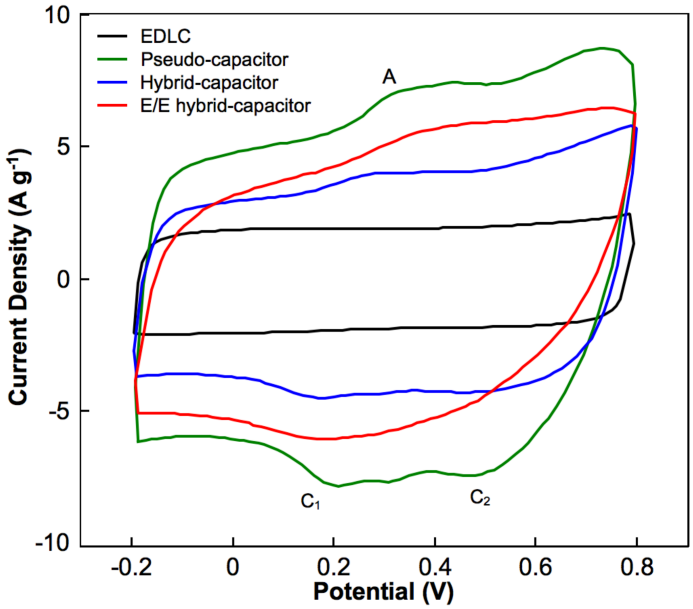

Figure 2.6 Capacitor performance (cyclic voltammetry) of EDLC (black), pseudo-capacitor (green), hybrid-capacitor (blue), and E/E hybrid-capacitor (red) at a scan rate of 100 mV s^{-1} in 1 M H_2SO_4 electrolyte at room temperature.

Figure 2.7 shows electrochemical performance of each capacitor with regard to galvanostatic charge-discharge measurements under 1 A g^{-1} in the potential range from 0 to 1 voltage. Figure 2.7(a) and 2.7(b) are the galvanostatic profiles after first charge-discharge cycle and 1000th charge-discharge cycle, respectively. Obvious IR drop can be observed in the discharging profiles. IR drop is defined as the electrical potential difference between the two ends of a conducting phase during a current flow and is the product of the current (I) and the resistance (R) of the conductor[57]. The IR drop can cause the energy loss during the charge-discharge performance, and can become significant under more number of cycles. The EDLC shows an isosceles triangular

profile without any obvious IR drop in both first and 1000th cycle. This performance of EDLC reveals excellent cycling stability for long cycling performance. From Figure 2.7(a), the pseudo-capacitor has longer discharge time based on the higher PANI ratio on the electrodes, however, it reveals the highest IR drop compared with other capacitors tested. This highest IR drop results in the largest energy loss after 1000th cycle charge-discharge in Figure 2.7(b), indicating the degradation of PANI during the charge-discharge performance. On the other hand, although the hybrid-capacitor and E/E hybrid-capacitor also show IR drops, the energy loss during the charge-discharge are much smaller compared to the pseudo-capacitor. This performance reflects the advantage of combining carbon materials with redox active materials that are common to pseudo-capacitors, which provides better cycling stability. The carbon materials can also provide lower internal resistance or improved conductivity between materials, therefore, less energy lost during the charge-discharge process[44].

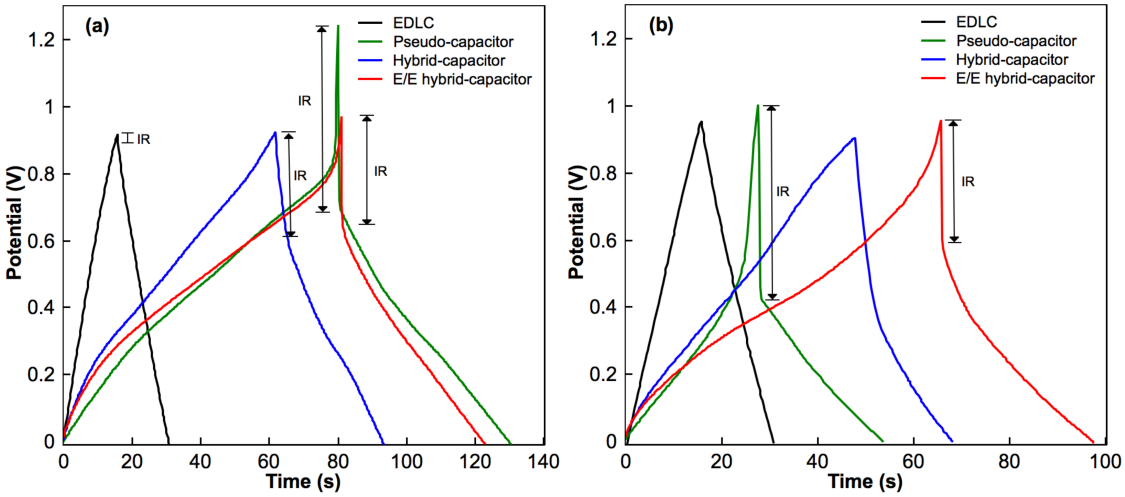

Figure 2.7 Capacitor performance (galvanostatic charge-discharge) of EDLC (black), pseudo-capacitor (green), hybrid-capacitor (blue), and E/E hybrid-capacitor (red) for (a) first cycle and (b) after 1000th cycle. 1 M H_2SO_4 electrolyte under current density of 1 A g^{-1} between potential range from 0 to 1 V at room temperature.

Table 2.1 listed the cell capacitance, energy density, and power density of the capacitors with control electrodes and E/E electrode. The PANI loading was measured with thermal gravimetric analysis (TGA). In the E/E hybrid-capacitor, the nanofiber structure appears to provides a larger surface area that results in faster ion diffusion (lower internal insistence) and higher charge storage that reflect is reflected in the higher specific capacitance (235.2 F g^{-1}). The power density of EDLC reveals the best power density (1.7 Wh g^{-1}) compared with the other capacitors as expected. There is also an improvement in power density for both hybrid-capacitor (1.6 Wh g^{-1}) and E/E hybrid-capacitor (1.4 Wh g^{-1}) compared to the pseudo-capacitor (1.3 Wh g^{-1}). These

observations reflect the improvement of power density due to the combination with carbon materials that match with other studies. [10,12,44]

Table 2.1 Capacitor performance.[a]

Capacitor Type	PANI (wt%)	Cell capacitance ($F\ g^{-1}$)	Energy density ($Wh\ g^{-1}$)	Power density ($kW\ g^{-1}$)
EDLC	0	66.4	7.5	1.7
Pseudo-capacitor	85	275.2	18.6	1.3
Hybrid-capacitor	59	138.1	14.3	1.6
E/E hybrid-capacitor	70	235.2	17.9	1.4

[a] performance calculated from galvanostatic charge-discharge data at a current density of 1 A g^{-1}.

2.3.3 Cycling Stability

The cycling stability was performed by using galvanostatic charge-discharge in potential range 0-0.9 V under 1000 cycles in order to understand the impact of electrode morphology on capacitor performance. The E/E hybrid-capacitor results are compared with control capacitors (EDLC, pseudo-capacitor, and hybrid-capacitor) under 1 A g^{-1} current density in 1 M H_2SO_4. The specific capacitance of different devices as a function of cycle number is shown in Figure 2.8. All of the capacitors show capacitance decay over the 1000 cycles. As expected, the EDLC and pseudo-capacitor reveals the lowest

and highest capacity decay, respectively. Interestingly, over the 1000 cycles, the E/E hybrid-capacitor (15.6 % loss) has a lower capacity decay compared to the hybrid-capacitor (32.7%). The stability results in Figure 2.8 indicate the impact of morphology in capacitor performance. The nanofiber structure appears to allow for a better distribution of both materials, where the distribution of carbon particles may reinforce or improve the mechanical stability of the PANI nanofibers and mitigate charge-discharge degradation.

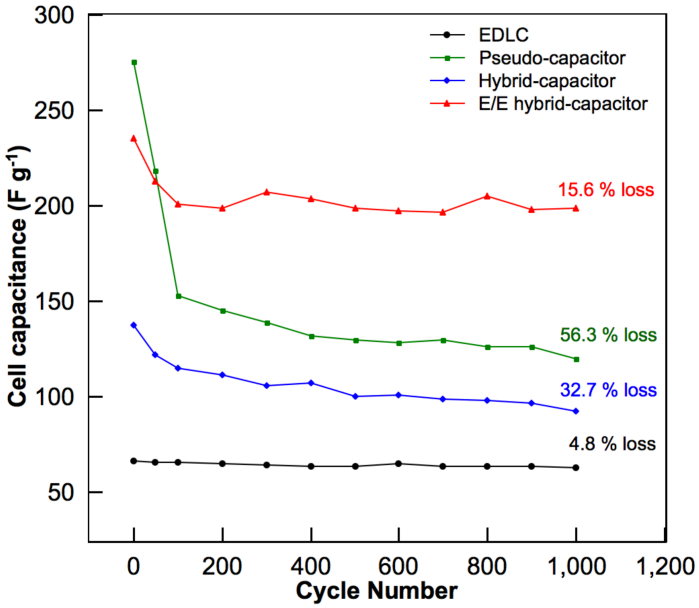

Figure 2.8 Cell capacitance of EDLC (black), pseudo-capacitor (green), hybrid-capacitor (blue), and E/E hybrid-capacitor (red) in 1 M H_2SO_4 electrolyte at current density of 1 A g^{-1} as a function of cycle number under room temperature.

2.3.4 *Post Mortem* SEM Images of Electrodes

Figure 2.9(a) and (b) show *post mortem* SEM images of E/E and solution casting PANI/carbon electrodes, respectively. In Figure 2.9(a), only a few fibers still remain in the electrode layer after the characterization testing. The compression and electrolyte penetration during the capacitor experiments alters the morphology of both PANI and carbon resulting in a modified nanostructure. Comparing 2.9(a) with 2.9(b), the *post mortem* E/E electrode has a higher porosity compared to the solution cast electrode. These remaining fiber and particle structure provide a rationale for the improved cycling stability in the E/E hybrid-capacitor compared to the hybrid-capacitor. However, few studies discuss the morphology of *post mortem* electrode structures in capacitor electrodes[50], which could be a critical factor in understanding capacitance degradation over many charge-discharge cycles. Further study and prevention of electrode degradation by combing PANI/carbon composite with different processes is currently underway.

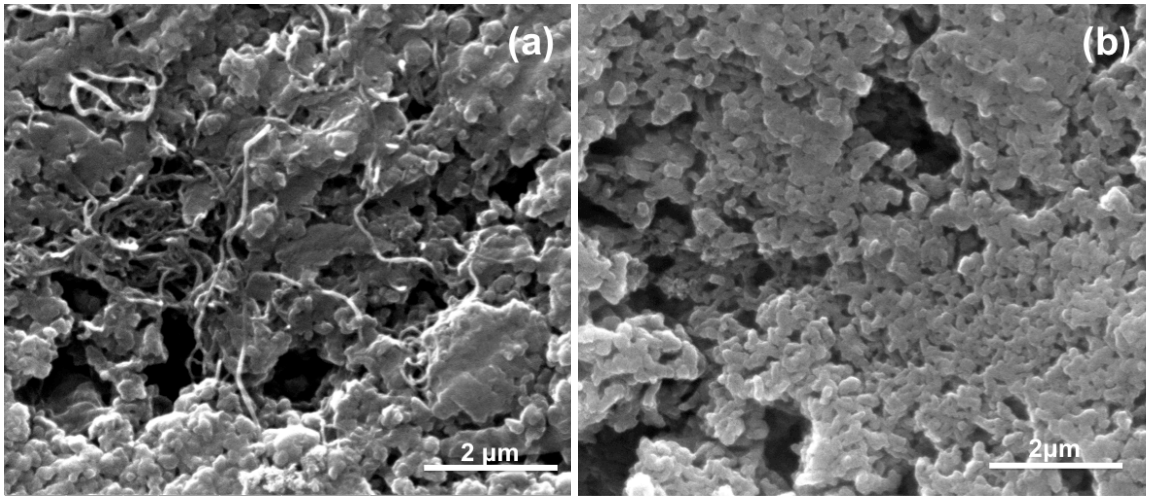

Figure 2.9 *post mortem* SEM images of (a) simultaneous electrospinning/electrospraying PANI/carbon electrode, X 30000 magnification, scale bar = 2 µm; (b) solution cast PANI/carbon electrode, X 30000 magnification, scale bar = 2 µm.

2.4 Conclusions

In this section, the simultaneous E/E technique shows the potential to produce an interconnected nanofiber/particle network hybrid electrode of PANI/carbon for hybrid-capacitors. The hybrid-capacitor with E/E electrodes displayed a higher specific capacitance (235 F g^{-1}) compared with a hybrid-capacitor with solution-cast hybrid electrodes (138.1 F g^{-1}). The nanofiber/particle network generated different morphology (porosity, surface area) that improved capacitance and cycling stability (84% compared to 67% retention over 1000 charge-discharge cycles when comparing capacitor with E/E electrodes to capacitor with solution-cast hybrid electrodes). This improvement in capacitance and stability in E/E electrodes demonstrates the feasibility of this processing technique, as well as potential in high-performance hybrid-capacitors.

3. *IN SITU* ELECTROCHEMICAL POLYMERIZATION OF CARBON NANOTUBE/POLYANILINE FOR HYBRID-CAPACITORS

3.1 Introduction

Carbon nanotubes (CNTs) have attracted interest due to their unique structure, chemical, mechanical, and electronic properties. They also have been studied as fillers for polymer composites.[58] Composites of CNTs and PANI have shown their potential in application to hybrid-capacitor. Due to their large aspect ratio and surface area, CNTs can serve as conducting bridge between the PANI domains.[59] Unlike the processing described in the previous section (a physical method to connect materials), in this section we focus on using a chemical method to covalently connect PANI to CNTs. CNTs/PANI composite can be synthesized chemically or electrochemically. Electrochemical methods, includes techniques such as electrochemical deposition. Chemical methods include surfactant-free aqueous polymerization, *in situ* oxidative polymerization, emulsion polymerization, and template directed polymerization.[15] In this study, we will fabricate multiwall carbon nanotube (MWCNT)/PANI composites via *in situ* oxidative polymerization.

3.1.1 *In situ* Polymerization for Synthesizing CNT/PANI Composites

Here we describe a review of previous work in this area. The *in situ* polymerization method is a polymerization process for preparing functional composites. This method

can produce polymer-grafted carbon nanotubes mixed with free polymer chains.[60] Cochet *et al.*[61] synthesized PANI/MWCNT composites by *in situ* polymerization. The Raman spectra and the transport measurements indicate a site-selective interaction between the polymer and the MWNTs facilitating the charge transfer processes. These results confirm that the formation of a true composite material with enhanced electronic properties. Wu *et al.*[62] analyzed the structure of *in situ* polymerized emeraldine salt PANI (PANI-ES) and carboxylic group functionalized multiwall carbon nanotubes (c-MWNTs) composites by scanning electron spectroscopy (SEM) and transmission electron spectroscopy (TEM). The images show that PANI-ES/c-MWNT composites are core (c-MWNT)-shell (doped-PANI-ES) tubular structure. (Figure 3.1 and Figure 3.2)

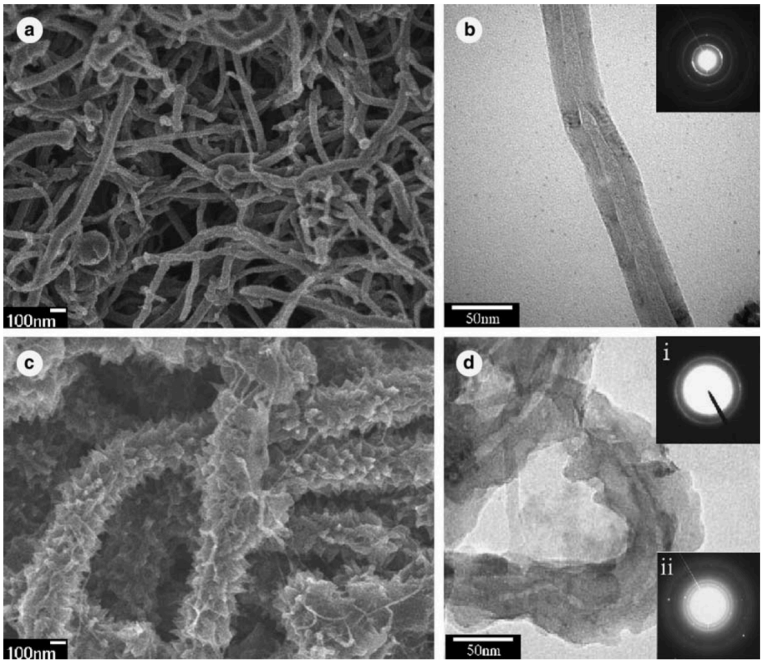

Figure 3.1 Field-emission scanning electron microscopy (FESEM) images of (a) c-MWNT and (b) 1 wt% MWNT-containing PANI-ES/c-MWNT composite. High-resolution transmission electron microscopy (HRTEM) and electron diffraction images of (c) c-MWNT and (d) 1 wt % MWNT-containing PANI-ES/c-MWNT composite (insert electron diffraction patterns of the PANI-ES/c-MWNT composites selected from the interface between the PANI and c-MWNT (pattern i) and the outer area of PANI (pattern ii)). Figure adopted from ref. [62].

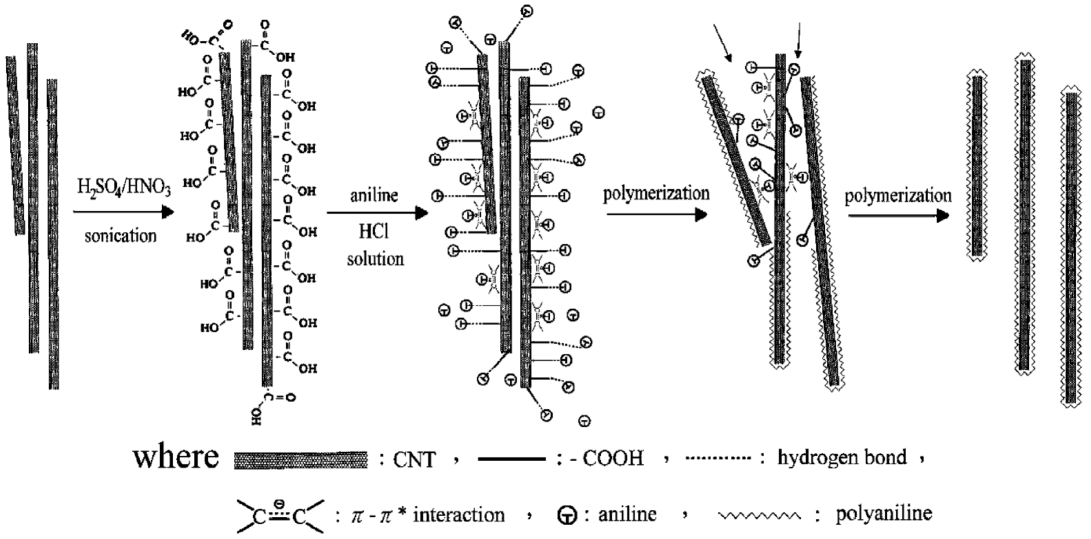

Figure 3.2 Schematic drawing of the mechanism governing the formation of PANI-ES/c-MWNT composites. Figure adopted from ref. [62].

Zang *et al.*[58] investigated the supercapactive behavior of *in situ* electrochemical polymerized MWCNT/PANI composite film. The results reveal that the MWCNT/PANI films show higher specific capacitance, better power performance, and better cycling ability, showing the MWCNT/PANI composite as a promising material for supercapacitor application (Figure 3.3).

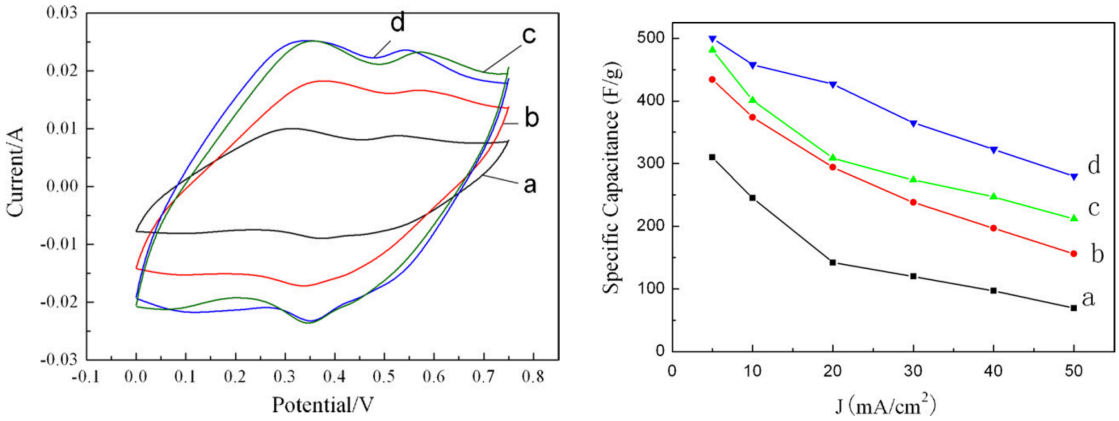

Figure 3.3 Voltammetric behavior (left) and specific capacitance (right) of the MWCNT/PANI composite films prepared from the growth solution with 0 (a), 0.2 (b), 0.4 (c) and 0.8 wt% (d) MWCNT. Figure adopted from ref. [58].

In order to obtain a uniform composite, the CNTs need to be homogeneously dispersed in the reacting solution. Various methods have been studied to disperse CNTs. In this study, we use functionalized multiwall carbon nanotubes (MWCNTs) to increase the interfacing binding between the MWCNTs and PANI. The functionalized MWCNTs are also easier to disperse in the solvent, producing a better dispersion and homogeneity of MWCNTs in the composite. The synthesis detail will be discussed in Section 3.2.2.

3.2 Experimental

3.2.1 Materials

Aniline (ACS reagent), chloroform (contains 100-200 ppm amylenes as stabilizer, ≥99.5%), ammonium persulfate (≥98%), hydrochloric acid (ACS reagent, 37%), and

sulfuric acid (ACS reagent, 95.0-98.0%), and sodium dodecylbenzenesulfonate (SDBS, technical grade) were purchased from Sigma-Aldrich and used as received. Polyethylene oxide (PEO, M_w = 8,000,000 g/mol, Polysciences, Inc.), multi-walled carbon nanotubes (MWCNTs)-COOH functionalized (>95%, OD: 10-20 nm, Length: 10-30 um, electrical conductivity: >100 s/cm, US4898, US Research Nanomaterials), porous separator (25μm microporous monolayer membrane (PP), 3501, Celgard), and untreated carbon fiber paper (165 μm measured by ultra meter caliper, EC-AC-Paper, FuelCell.com) were used as received. All solutions used in this study were made using deionized water obtained from a NANOPure water purification system (Barnstead) with the resistivity greater than 18 MΩ·cm (25 °C).

3.2.2 Synthesis of Multiwall Carbon Nanotube/Polyaniline Composite

MWCNT-PANI composite was synthesized by *in situ* polymerization using a procedure similar to one reported in the literature.[62] The 1:1 w/w (to aniline monomers) of COOH-functionalized MWCNTs were dispersed in a well-stirred 1 M HCl solution for over 3 h. 0.25 M aniline monomers were then added and the solutions was transferred to a three neck flask submerged in an ice bath. In another flask, 0.25 M ammonium persulfate (APS) in 1 M HCl was prepared. APS solution was then slowly added dropwise (3 drops per minute) into a well-stirred MWCNT solution at 0 °C. The reaction mixing solution was stirred for 2 h at 0 °C. The final product should be a dark green/black color indicating the MWCNT and emeraldine salt of PANI. After polymerization, the solution was collected and purified and mixed in deionized water for

6 h. MWCNT/PANI powder was obtained after filtering and drying under dynamic vacuum at 60 °C for 24 h.

3.2.3 Fabrication of MWCNT-PANI Electrodes for Capacitors

MWCNT and MWCNT-PANI electrodes were fabricated by solution casting onto carbon fiber paper. The cast solution was prepared by adding MWCNT-PANI to chloroform at 0.7% w/w with 1:1 w/w surfactant sodium dodecylbenzenesulfonate (SDBS) and sonicating at an amplitude of 35% for 15 min. The MWCNT electrode (control) was also prepared by the same method. Solutions were transferred from a glass pipet and uniformly drop cast on 3 x 3 cm carbon fiber paper coupons. The solution-cast samples were then annealed at 80 °C for 5 min. Additional layers were solution cast and annealed until the desired loading of active material of at least 4 mg cm^{-1} was reached. After solution casting the desired amount, all control electrodes were further annealed at 120 °C for 90 min prior to capacitor assembly.

3.2.4 Fabrication of Electrodes for Capacitors *via* Simultaneous Electrospinning/Electrospraying (E/E)

The solution for electrospinning was prepared by dissolving PANI in chloroform at 0.67% w/w followed by stirring for 24 h to ensure a clear uniform homogeneous solution. Polyethylene oxide (PEO) was then added to the solution at 0.1% w/w and stirred for 1 h to ensure a uniform solution prior to electrospinning. The electrospraying solution was

prepared by adding MWCNT-PANI and same weight amount of surfactant (sodium dodecylbenzenesulfonate, SDBS) to chloroform at 1.4% w/w. The solution was then sonicated (125 W, 20 kHz) at an amplitude of 35% for 15 min. The electrospraying MWCNT solution (control) was also prepared in the same way. Both solutions were placed in two separate glass syringes. The solution flow rates, the needle tip to collector distance, and the applied voltage for electrospinning and electrospraying process were 0.8 ml/hr and 1 ml/hr, 7 cm and 10 cm, and 7 kV and, 8 kV, respectively. The comparative hybrid-capacitor control electrodes were fabricated by solution casting a PANI/MWCNT-PANI solution onto carbon fiber paper similar to the method in Section 3.2.3. The PANI/MWCNT-PANI solution was a combination of the solutions previously described above (similar to electrospinning and electrospraying solutions). The electrodes were subsequently annealed at 120 °C for 90 min.

3.2.5 Characterization

The morphology of the MWCNT/PANI composite and E/E electrode were characterized by transmission electron microscopy (TEM, JEOL JEM-2010 TEM, 200kV) and scanning electron microscopy (SEM; FEI Quanta 600 FE-SEM, 10-20 kV). The TEM samples were prepared by sonication in chloroform. The homogeneously dispersed solution then solution cast on copper grid (lacey carbon coated, 200 mesh, 3mm, 3820C-CF, SPI Supplies.). SEM samples were sputter coated (Cressington 208 HR) with platinum (6 nm thickness) prior to SEM. The specific MWCNT/PANI loading was measured with thermal gravimetric analysis (TGA; Q50, TA Instrument). A small

portion of the sample (*ca.* 5 - 7 mg) was heated in the TGA from ambient temperature to 900 °C at 10 °C/min in air at 60 ml/min. The PANI and MWCNT loading were calculated by dividing the mass loss by the entire original material mass. The capacitor assembly and performance testing (cyclic voltammetry, galvanostatic charge-discharge) are following the same methods discussed in sections 2.2.5 and 2.2.6, respectively.

3.3 Results and Discussion

3.3.1 Microstructure Characterization

To confirm the nanostructures, Figure 3.4(a) and (b) show the TEM images of MWCNTs and MWCNT-PANI composites, respectively. Figure 3.4(c) and (d) are magnified views of (a) and (b), respectively. All four images show the hollow inside structures with tubular layers for MWCNTs. From the images, the MWCNTs reveal two layers (first black layer and second white layer from the MWCNT outer surface). The average diameter size of MWCNTs in Figure 3.4(a) is 23.3 nm (diameter range from 20 to 25 nm). The diameter of MWCNT-PANI composites are larger with an average diameter 29.3 nm (diameter range from 28 to 33 nm). We hypothesize that the PANI macromolecules encapsulate the outer surface of the MWCNTs resulting in a larger diameter for the MWCNTs. The MWCNT-PANI composites form core-shell structure, while the MWCNTs serve as the core with PANI covalently attached to the surface. However, the ability to clearly distinguish the surface morphology is limited by the TEM technique used. The microstructure of PANI and its uniformity are unknown in these

images. The future investigation will focus on using high-resolution TEM to determinate the surface morphology of MWCNT-PANI composites.

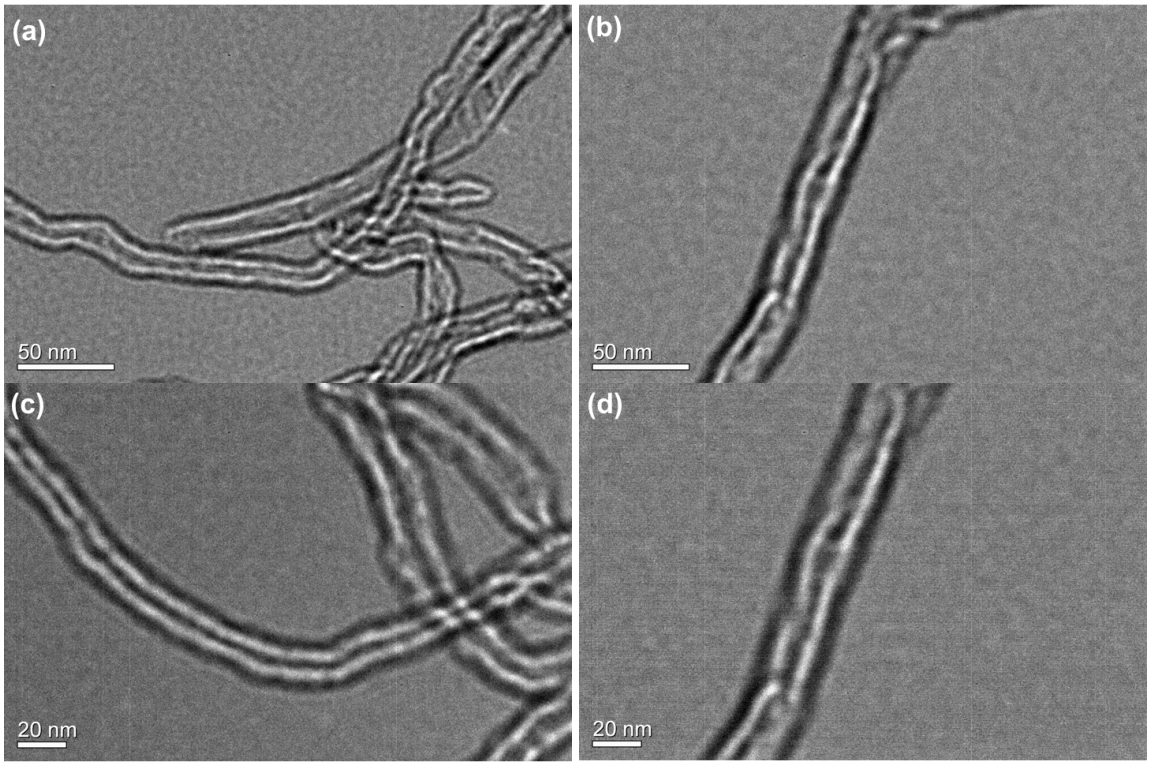

Figure 3.4 TEM images of (a) MWCNT and (b) MWCNT-PANI at X 80000 magnification, scale bar = 50 nm.; magnified TEM images of (c) MWCNT and (d) MWCNT-PANI at X 100000 magnification, scale bar = 20 nm.

3.3.2 Thermal Gravimetric Analysis (TGA)

The composition of MWCNT-PANI composite were analyzed by thermogravimetric curves (TGA curves). Figure 3.5 shows the comparison of mass losses of MWCNT,

PANI and MWCNT (50wt%)-PANI upon heating in air from 25 to 900 °C. MWCNT is thermally stable in the range of 25 to 550 °C. The intense increasing of weight loss starts at 600 °C until the end of the heating process. For pure PANI and MWCNT-PANI samples, the weight loss can be divided into three major stages at 100, 300 and 500 °C. The main weight loss below 100 °C is assigned evaporation of water from the samples. For pure PANI, a steady decrease of weight starts at 200 to 300 °C, indicating the release of acid dopant from PANI, suggesting a de-doping process has occurred in this range. After this, a significant weight loss around 500 °C was observed and can be attributed to the polymer decomposition. At 600 °C, PANI loses approximately 95.8 % of its weight. For the MWCNT-PANI composite, the weight loss shows a similar trend compare to pure PANI before 600 °C; however, the degradation of MWCNT-PANI after 600 °C indicates a residue ratio of 39.4 %, which correspond to the remaining MWCNT. Therefore, comparing the different patterns between pure PANI and MWCNT-PANI, the real loading of PANI in the MWCNT-PANI composite was determined to be 65 wt%.

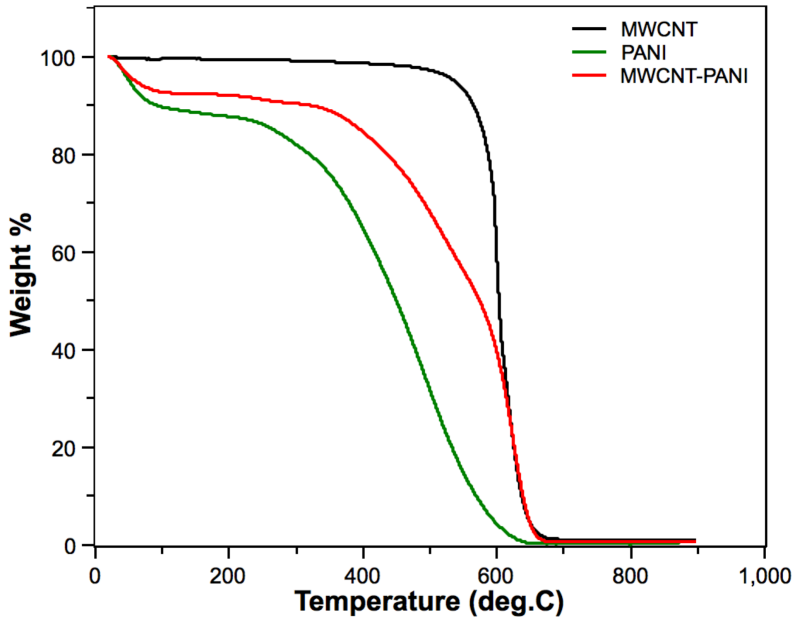

Figure 3.5 Thermal gravimetric analysis (TGA) of MWCNT (black), PANI (green), and MWCNT-PANI composite (red).

3.3.3 Electrochemical Performance of Capacitors with MWCNT-PANI Electrodes

In order to evaluate the electrochemical properties of MWCNT-PANI composites in a capacitor, the cyclic voltammetry (CV) and galvanostatic charge-discharge of a capacitor with solution-cast MWCNT-PANI electrodes were measured with 1 M H_2SO_4 as the electrolyte. The results were also compared with solution-cast MWCNT electrodes. Figure 3.6(a) shows the CV profiles of two capacitors at a 100 mV s^{-1} scan rate in potential range -0.2 V to 0.8 V. The capacitor with pure MWCNT electrodes shows a partial rectangular profile with redox peaks at 0.05/-0.02 V. These two redox peaks can assigned to the presence of oxygen-containing groups (functionalized carboxylic acid group) bound to the surface of carbon nanotubes and agree with previous literature.[63,64]

Conversely, the capacitor with MWCNT-PANI electrodes shows a curve similar to the E/E hybrid-capacitor behavior in section 2.3.2 with two pairs of redox peaks corresponding to the transition of PANI between emeraldine/leucoemeraldine and emeraldine/pernigraniline. The MWCNT-PANI also exhibits higher current density, attributing to the PANI contents. Figure 3.6(b) shows electrochemical performance of the two capacitors in reference to galvanostatic charge-discharge measurements under 1 A g^{-1}. The capacitor with MWCNT-PANI electrodes displays an obvious IR drop and compares with the triangular profile of MWCNT electrodes. The capacitor with the MWCNT-PANI electrodes also reveals a longer discharge time, providing much higher capacitance (55.1 F g^{-1}) compared with the capacitor with MWCNT electrodes (11.7 F g^{-1}). This performance matches our expectation that the chemically bonded PANI in the MWCNT-PANI composites can provide a synergistic effect; the PANI on MWCNT tubular surface provides a pseudo-capacitive mechanism and increases the specific capacitance.

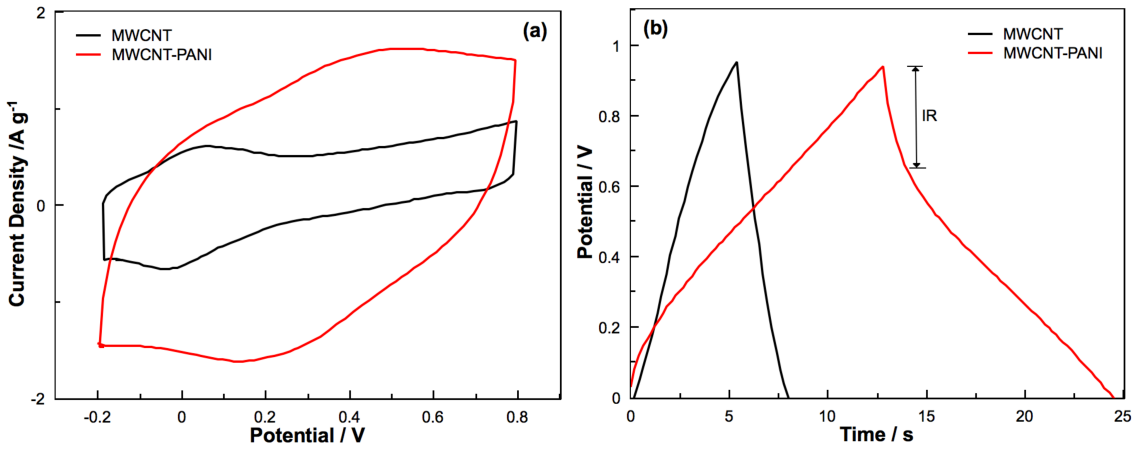

Figure 3.6 Capacitor performance with MWCNT electrodes (black) and MWCNT-PANI electrodes (red): (a) cyclic voltammetry at a scan rate of 100 mV s^{-1} in 1 M H_2SO_4 electrolyte and (b) galvanostatic charge-discharge with 1 M H_2SO_4 electrolyte under a current density of 1 A g^{-1} between potential range from 0 to 1 V at room temperature.

3.3.4 Electrochemical Performance of Capacitors with Electrodes Produced *via* Simultaneous Electrospinning/Electrospraying (E/E)

PANI/MWCNT-PANI composite electrodes were fabricated *via* simultaneous electrospinning/electrospraying (E/E) for hybrid-capacitors. Electrochemical performance of the hybrid-capacitor with E/E PANI/MWCNT-PANI electrodes was measured with cyclic voltammetry and galvanostatic charge-discharge tests in 1 M H_2SO_4 electrolyte. The electrochemical results were compared to control capacitors: capacitors with E/E PANI/MWCNT electrodes and solution-cast PANI/MWCNT electrodes. All the testing cells were assembled with a symmetric structure in a split test cell with two 1.57 cm^2 electrodes. Figure 3.7 shows the CV profiles of all three

capacitors at a 100 mV s^{-1} scan rate in the potential range -0.2 V to 0.8 V. All three hybrid-capacitors show the redox behavior of a typical pseudo-capacitance performance. The solution-cast MWCNT/PANI electrodes show the most distinct two pairs of redox peaks (A/C_1 and A/C_2) corresponding to the transition of PANI that matched with the previous discussion in Section 2.3.2. The two E/E electrodes exhibit larger current density compared with solution-cast one, corresponding with our E/E performance in Section 2. However, these two capacitors show similar cyclic voltammograms, which might relate to the PANI loading. Also, the capacitor with E/E PANI/MWCNT-PANI electrodes reveals more pseudo-capacitive behavior with more distinct two pairs of redox peaks, indicating a more effective connection between PANI and MWCNT.

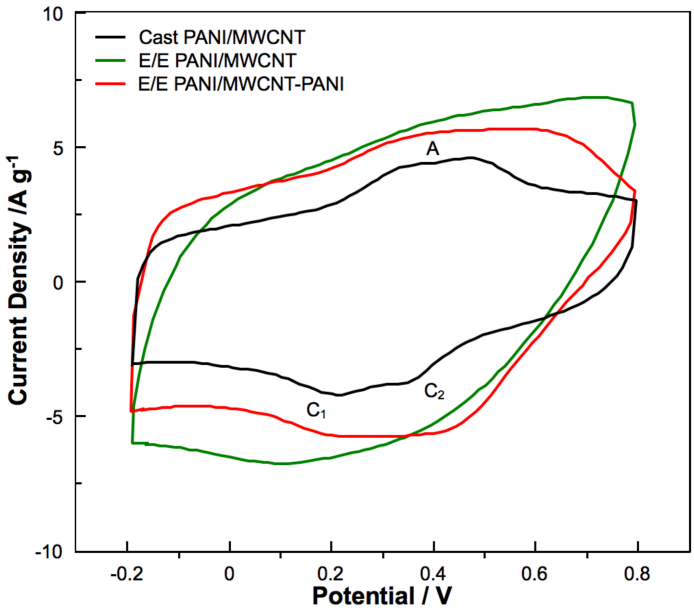

Figure 3.7 Capacitor performance (cyclic voltammetry) with cast PANI/MWCNT electrodes (black), E/E PANI/MWCNT electrodes (green), and E/E PANI/MWCNT-PANI electrodes (red) at a scan rate of 100 mV s^{-1} in 1 M H_2SO_4 electrolyte at room temperature.

Fig. 3.8 shows the electrochemical performance of each capacitor with regards to galvanostatic charge-discharge measurements under 1 A g^{-1} in the potential range from 0 to 1 V. All three capacitors exhibit the IR drop in the discharge profiles, corresponding with the hybrid-capacitor performance shown in Figure 2.7. The two capacitors with E/E electrodes have longer discharge times compare with the capacitor with solution-cast electrodes, suggesting the advantage of morphology change by the E/E processing. However, the capacitor with the E/E PANI/MWCNT electrodes has an approximately 10 seconds longer discharge time compared to the capacitor with the E/E PANI/MWCNT-

PANI electrodes and this conflicts with our expectations. In our previous hypothesis, the MWCNT-PANI should improve the electrode capacitance and stability by their compact chemical bonding. We conclude reasons that might cause this difference: (1) the specific PANI loading through the E/E process is not uniform on both electrodes, (2) the higher PANI loading through the E/E process could decrease the MWCNT-PANI performance, and (3) the improved cycling stability cannot be detected by short cycling. Further investigations should focus on thermal gravimetric analysis (TGA) and cycling stability testing for a thorough specific PANI loading and cycling stability. Also, diverse fabricating techniques can be developed and improved for hybrid-capacitors, creating a more effective way to blend multiple materials.

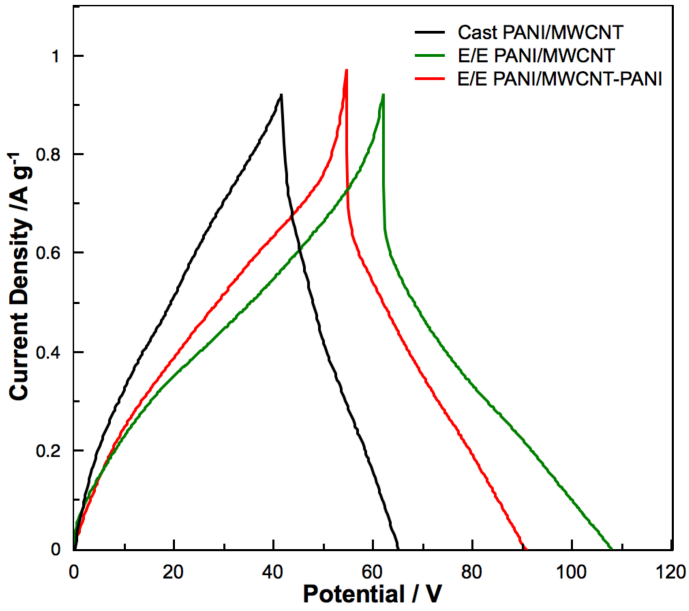

Figure 3.8 Capacitor performance (galvanostatic charge-discharge) with cast PANI/MWCNT electrodes (black), E/E PANI/MWCNT electrodes (green), and E/E PANI/MWCNT-PANI electrodes (red). 1 M H_2SO_4 electrolyte under current density of 1 A g^{-1} between potential range from 0 to 1 V at room temperature.

3.4 Conclusions

In this section, the *in situ* polymerized MWCNT-PANI composites show improved electrochemical performance in a capacitor compared with pure MWCNTs due to the compact chemical bonding between MWCNT and PANI. MWCNT-PANI composite electrodes were then produced *via* simultaneous E/E technique for hybrid-capacitors. This hybrid-electrode displays a higher performance compared with solution-cast hybrid-electrode. However, the cyclic voltammetry and galvanostatic charge-discharge tests between E/E PANI/MWCNT and E/E PANI/MWCNT-PANI electrodes show little

difference between them. The future works will focus on: (1) further investigation of MWCNT-PANI composites with high-resolution TEM, TGA, and cycling stability, (2) other processing methods at different MWCNT to PANI w/w ratios.

4. SUMMARY AND FUTURE OUTLOOK

4.1 Summary

This work demonstrates the fabrication and characterization of PANI/carbon electrodes for application to supercapacitors. Two fabricating processes for PANI/carbon electrodes were investigated: simultaneous electrospinning/electrospraying (E/E) and *in situ* polymerization. The surface morphologies and electrochemical performance (e.g. cyclic voltammetry, galvanostatic charge-discharge, and cycling stability) of hybrid capacitors with these electrodes were investigated.

The E/E technique shows the potential to produce an interconnected nanofiber/particle network hybrid electrode of PANI/carbon for hybrid-capacitors. The nanofiber/particle network generated a unique morphology (porosity, surface area) that improved capacitance and cycling stability. In another study, a composite of MWCNTs and PANI were produced *via in situ* polymerization technique. The MWCNT-PANI electrode presents distinct redox peaks and enhanced performance, showing the synergistic effect of adding PANI. Hybrid-capacitors with E/E PANI/MWCNT-PANI were also investigated. The results from this thesis show that capacitor performance has a high correlation with electrode morphology and carbon-polymer interfaces that can be modified by fabrication and synthetic processes.

4.2 Future Outlook

Beyond this study, several possibilities exist for expanding on this work. In this study, we only focused on adjusting material morphology and structure to facilitate the electrode performance. Since only the electrochemical performance (*e.g.* cyclic voltammetry and galvanostatic charge-discharge) under various nanostructures were studied, the detailed molecular mechanisms of charge storage in these capacitors remain vague. Many efforts have focused on developing new materials that can store more charge; however, the success of this approach requires an understanding of the material structure and how this can affect the charge storage mechanism.[65]

In situ characterization methods, such as nuclear magnetic resonance (NMR) spectroscopy, electrochemical quartz crystal microbalance (EQCM), infrared (IR) spectroscopy, and scattering approaches (SAXS and SANS) have recently been designed to study the electrochemical charge storage mechanisms on a nanometer and molecular level. The traditional explanation for electric double layer capacitor states that the charge accumulates in the electric double layer near the electrode/electrolyte surface; however, the ion diffusion or migration may change with highly porous electrodes (*i.e.*, electrodes with 2D or 3D structures). Therefore, different charging mechanisms for ion adsorption, desorption, and exchange may go beyond the traditional view of capacitor mechanism and require more thorough consideration.

Recent studies of charge storage within the porous carbons (*e.g.,* activated carbon) have led to an improved understanding of non-Faradaic ion exchange mechanism. Carbon with its diverse materials (*e.g.,* carbon nanotubes and graphenes) also need

detailed analysis. Therefore, it is necessary to consider supercapacitors with Faradaic reactions (*i.e.*, pseudo-capacitors and hybrid-capacitors). These capacitors include both chemical reaction and ion adsorption/desorption and require a different design for the characterization techniques. Kellenberger *et al*.[66] investigated the doping mechanisms of PANI by *in situ* Fourier transform infrared (FTIR) spectroelectrochemistry using attenuated total reflection (ATR). The formation of charged states in PANI can be studied *via* changes in IR bands under a potential, giving a detailed understanding of the electrochemical oxidation process. Further characterization is necessary to explain the factors that control charge storage mechanism in hybrid materials and a connection between mechanisms and capacitor performance. A fundamental understanding of charge storage mechanisms in hybrid materials will allow for a targeted design of new hybrid materials for enhanced capacitor performance.

REFERENCES

(1)Simon, P.; Gogotsi, Y. *Nature Materials* **2008**, *7*, 845

(2)Snook, G. A.; Kao, P.; Best, A. S. *J. Power Sources* **2011**, *196*, 1.

(3)Obreja, V. V. N. *Physica E: Low-dimensional Systems and Nanostructures* **2008**, *40*, 2596.

(4)Aiping Yu , V. C., and Jiujun Zhang *Electrochemical Supercapacitors for Energy Storage and Delivery Fundamentals and Applications*; CRC Press, **2013**.

(5)Conway, B. E. *Electrochemical supercapacitors: scientific fundamentals and technological applications*; Springer Science & Business Media., **1999**.

(6)Conway, B. E.; Pell, W. G. *J. Solid State Electrochem.* **2003**, *7*, 637.

(7)Yu, G.; Xie, X.; Pan, L.; Bao, Z.; Cui, Y. *Nano Energy* **2013**, *2*, 213.

(8)Shown, I.; Ganguly, A.; Chen, L.-C.; Chen, K.-H. *Energy Science & Engineering* **2015**, *3*, 2.

(9)Naoi, K.; Simon, P. *J. Electrochem. Soc.* **2008**, *17*, 34.

(10)Wang, K.; Zhao, P.; Zhou, X.; Wu, H.; Wei, Z. *J. Mater. Chem.* **2011**, *21*, 16373.

(11)Yan, X.; Tai, Z.; Chen, J.; Xue, Q. *Nanoscale* **2011**, *3*, 212.

(12)Wang, T.; Wang, W.; Dai, Y.; Zhang, H.; Shen, Z.; Chen, Y.; Hu, X. *Russ. J. Electrochem.* **2014**, *51*, 743.

(13)Tran, C.; Singhal, R.; Lawrence, D.; Kalra, V. *J. Power Sources* **2015**, *293*, 373.

(14)Asturias, G. E.; MacDiarmid, A. G.; McCall, R. P.; Epstein, A. J. *Synth. Met.* **1989**, *29*, 157.

(15)Oueiny, C.; Berlioz, S.; Perrin, F.-X. *Prog. Polym. Sci.* **2014**, *39*, 707.

(16)Li, D.; Huang, J.; Kaner, R. B. *Acc. Chem. Res.* **2008**, *42.1*, 135.

(17)DeBerry, D. W. *J. Electrochem. Soc.* **1985**, *132*.

(18)S, P., Sitaram, ; J, O., Stoffer,; T, J., O'Keefe *Journal of Coatings Technology* **1997**, *69*, 65.

(19)N. Gospodinova; Terlemezyan, L. *Prog. Polym. Sci.* **1998**, *23*, 1443.

(20)Huang, J.; Kaner, R. B. *J. Am. Chem. Soc.* **2004**, *126*, 851.

(21)Wu-Song Huang; Humphrey, B. D.; MacDiarmid, A. G. *J. Chem. Soc., Faraday Trans.* **1986**, *82*, 2385.

(22)Zhang, D.; Wang, Y. *Materials Science and Engineering: B* **2006**, *134*, 9.

(23)Chen, W.; Xia, C.; Rakhi, R. B.; Alshareef, H. N. *J. Power Sources* **2014**, *267*, 521.

(24)Simon, P.; Gogotsi, Y. *Acc. Chem. Res.* **2012**, *46*, 1094.

(25)Miao, J.; Miyauchi, M.; Simmons, T. J.; Dordick, J. S.; Linhardt, R. J. *Journal of Nanoscience and Nanotechnology* **2010**, *10*, 5507.

(26)Deitzel, J. M.; Kleinmeyer, J.; Harris, D.; Tan, N. C. B. *Polymer* **2001**, *42*, 261.

(27)Song, T.; Chen, Z.; He, H.; Liu, Y.; Liu, Y.; Ramakrishna, S. *J. Appl. Polym. Sci.* **2015**, *132*.

(28)Ballengee, J. B.; Pintauro, P. N. *J. Electrochem. Soc.* **2011**, *158*, B568.

(29)Hong Chen, J. D. S., and Yossef A. Elabd **2007**.

(30)Kim, C. *J. Power Sources* **2005**, *142*, 382.

(31)Zhi, M.; Liu, S.; Hong, Z.; Wu, N. *RSC Adv.* **2014**, *4*, 43619.

(32)Ian D. Norris; Manal M. Shaker; Frank K. Ko; MacDiarmid, A. G. *Synth. Met.* **2000**, *114*, 109.

(33)Zhou, Z.; Wu, X.-F. *J. Power Sources* **2013**, *222*, 410.

(34)Ramakrishna, S.; Fujihara, K.; Teo, W.-E.; Yong, T.; Ma, Z.; Ramaseshan, R. *Mater. Today* **2006**, *9*, 40.

(35)Greiner, A.; Wendorff, J. H. *Angew. Chem. Int. Ed. Engl.* **2007**, *46*, 5670.

(36)Heineman, P. T. K. a. W. R. *J. Chem. Educ.* **1983**, *60*.

(37)Bard, A. J.; Faulkner, L. R.; Leddy, J.; Zoski., C. G. *Electrochemical methods: fundamentals and applications*; New York: Wiley, **1980**; Vol. 2.

(38)NICHOLSON, R. S. *Anal. Chem.* **1965**, *37*, 1351.

(39)Mabboil, G. A. *J. Chem. Educ.* **1983**, *6*, 697.

(40)MacDiarmid, A. G.; Yang, L. S.; Huang, W. S.; Humphrey, B. D. *Synth. Met.* **1987**, *18*, 393.

(41)Shen-Ming Chen, R. R., Veerappan Mani, Ramiah Saraswathi *International Journal of Electrochemical Science* **2014**.

(42)Ketabi, S.; Le, Z.; Lian, K. *Electrochem. Solid-State Lett.* **2011**, *15*, A19.

(43)Pandey, G. P.; Rastogi, A. C. *J. Electrochem. Soc.* **2012**, *159*, A1664.

(44)Wu, Q.; Xu, Y.; Yao, Z.; Liu, A.; Shi, G. *ACS Nano* **2010**, *4*, 1963.

(45)Huang, Z.-M.; Zhang, Y. Z.; Kotaki, M.; Ramakrishna, S. *Compos. Sci. Technol.* **2003**, *63*, 2223.

(46)Miao, Y. E.; Fan, W.; Chen, D.; Liu, T. *ACS applied materials & interfaces* **2013**, *5*, 4423.

(47)Wu, J.; Wang, N.; Zhao, Y.; Jiang, L. *Journal of Materials Chemistry A* **2013**, *1*, 7290.

(48)Zhi, M.; Manivannan, A.; Meng, F.; Wu, N. *J. Power Sources* **2012**, *208*, 345.

(49)Kim, C.; Yang, K. S. *Appl. Phys. Lett.* **2003**, *83*, 1216.

(50)Wang, X.; Richey, F. W.; Wujcik, K. H.; Elabd, Y. A. *J. Power Sources* **2014**, *264*, 42.

(51)Wang, X.; Richey, F. W.; Wujcik, K. H.; Ventura, R.; Mattson, K.; Elabd, Y. A. *Electrochim. Acta* **2014**, *139*, 217.

(52)Santos, M. C.; Elabd, Y. A.; Jing, Y.; Chaplin, B. P.; Fang, L. *AlChE J.* **2016**, *62*, 508.

(53)Vivier, V.; Cachet-Vivier, C.; Regis, A.; Sagon, G.; Nedelec, J. Y.; Yu, L. T. *J. Solid State Electrochem.* **2002**, *6*, 522.

(54)Sivakkumar, S. R.; Kim, W. J.; Choi, J.-A.; MacFarlane, D. R.; Forsyth, M.; Kim, D.-W. *J. Power Sources* **2007**, *171*, 1062.

(55)Genies, E. M.; Tsintavis, C. *Journal of Electroanalytical Chemistry and Interfacial Electrochemistry* **1985**, *195*, 109.

(56)Chaudhari, S.; Sharma, Y.; Archana, P. S.; Jose, R.; Ramakrishna, S.; Mhaisalkar, S.; Srinivasan, M. *J. Appl. Polym. Sci.* **2013**, *129*, 1660.

(57)Subramanian, V.; Zhu, H.; Wei, B. *Electrochem. Commun.* **2006**, *8*, 827.

(58)Zhang, J.; Kong, L.-B.; Wang, B.; Luo, Y.-C.; Kang, L. *Synth. Met.* **2009**, *159*, 260.

(59)Kim, D. K.; Wha Oh, K.; Kim, S. H. *J. Polym. Sci., Part B: Polym. Phys.* **2008**, *46*, 2255.

(60)Spitalsky, Z.; Tasis, D.; Papagelis, K.; Galiotis, C. *Prog. Polym. Sci.* **2010**, *35*, 357.

(61)Cochet, M.; Maser, W. K.; Benito, A. M.; Callejas, M. A.; Martínez, M. T.; Benoit, J.-M.; Schreiber, J.; Chauvet, O. *Chem. Commun.* **2001**, 1450.

(62)Wu, T.-M.; Lin, Y.-W.; Liao, C.-S. *Carbon* **2005**, *43*, 734.

(63)Barisci, J. N.; Wallace, G. G.; Baughman, R. H. *J. Electrochem. Soc.* **2000**, *147*, 4580.

(64)Chen, Q.-L.; Xue, K.-H.; Shen, W.; Tao, F.-F.; Yin, S.-Y.; Xu, W. *Electrochim. Acta* **2004**, *49*, 4157.

(65)Forse, A. C.; Merlet, C.; Griffin, J. M.; Grey, C. P. *J. Am. Chem. Soc.* **2016**, *138*, 5731.

(66)Kellenberger, A.; Dmitrieva, E.; Dunsch, L. *J. Phys. Chem. B* **2012**, *116*, 4377.